

Size-selected black carbon mass distributions and mixing state in polluted and clean environments of northern India

Tomi Raatikainen¹, David Brus¹, Rakesh K. Hooda^{1,2}, Antti-Pekka Hyvärinen¹, Eija Asmi¹, Ved P. Sharma², Antti Arola³, and Heikki Lihavainen¹

¹Finnish Meteorological Institute, Helsinki, Finland

²The Energy and Resources Institute, Delhi, India

³Finnish Meteorological Institute, Kuopio, Finland

Correspondence to: T. Raatikainen (tomii.raatikainen@fmi.fi)

Abstract. We have measured black carbon properties by using a size-selected Single Particle Soot Photometer (SP2). The measurements were conducted in northern India at two sites: Gual Pahari is located at the Indo-Gangetic plains (IGP) and Mukteshwar at the Himalayan foothills. Northern India is known as one of the absorbing aerosol hot spots, but detailed information about absorbing aerosol mixing state is still largely missing. Previous ~~black-carbon-equivalent~~ black carbon (eBC) mass concentration measurements are available for this region and these are consistent with our observations showing that refractory black carbon (rBC) concentrations are about ten times higher in Gual Pahari than those at Mukteshwar. Also the number fraction of ~~absorbing-rBC-containing~~ particles is higher in Gual Pahari, but individual ~~absorbing-particles-including-rBC-containing~~ particles and their size distributions are fairly similar. These findings indicate that particles at both sites have similar local and regional emission sources, but aerosols are also transported from the main source regions (IGP) to the less polluted regions (Himalayan foothills). Detailed examination of the ~~absorbing-rBC-containing~~ particle properties revealed that they are most likely ~~irregular particles such as~~ fractal aggregates, but the exact structure remains unknown.

1 Introduction

Absorbing aerosols are warming the global climate, but uncertainties are still significant partly due to the lack of detailed experimental data on aerosol spatial and temporal distributions and their physical properties (Stocker et al., 2013; Bond et al., 2013). Broadly defined black carbon (BC) is typically the main absorbing aerosol component in submicron aerosols and its radiative effects depend on absolute concentrations and mixing state, which describes how BC is distributed within the aerosol particles (Bond and Bergstrom, 2006; Petzold et al., 2013; Lack et al., 2014). Although ~~total-BC~~ mass concentrations ~~can-be-routinely-are-often~~ measured, the information about the mixing state ~~and-size-distribution-of-BC~~ is currently limited. ~~Freshly-For~~ some sources the freshly emitted BC can be almost pure ~~elemental-black~~ carbon, but rapid atmospheric processing leads to mixed particles containing significant mass fractions of other typical aerosol species such as sulphate and organics. The inclusion of non-absorbing components may cause an increase to BC absorption by a so-called lensing effect, but this also depends on the structure of the particle (~~e.g., Adachi et al., 2010; Cappa et al., 2012; Peng et al., 2016~~). ~~Spherical-BC-core-coated-by-the-non-absorbing-material-is-a-major-simplification-for-the-particle-structure-~~ (e.g., Adachi et al., 2010; Cappa et al.,

2012; He et al., 2015; Peng et al., 2016). In addition to the direct radiative effect, aerosol water uptake depends ~~strongly~~ on the volume fraction of soluble aerosol species as pure BC is hydrophobic. Some absorbing aerosol particles can act as a cloud condensation nuclei (CCN), which means that ~~that~~ BC can have an effect on cloud properties (an indirect climate effect) ~~and that BC can participate in cloud processing~~. Therefore, knowing the ~~BC~~ mixing state is highly important when assessing the
5 climate effects of BC.

Recent development of single particle instruments capable of detecting BC (e.g., Cross et al., 2010; Lack et al., 2014) has provided detailed information about the BC mixing state. One widely used instrument for this purpose is the Single Particle Soot Photometer, SP2, (Stephens et al., 2003; Schwarz et al., 2006; Moteki and Kondo, 2007) developed by Droplet Measurement ~~Techniques-Technologies~~ (Boulder, CO, USA). This instrument uses laser induced incandescence technique to detect so-called
10 refractory black carbon (rBC), which is the fraction of the absorbing carbonaceous material that has boiling point close to 4000 K and ~~therefore~~, emits visible light when heated to that temperature (Petzold et al., 2013; Lack et al., 2014). The rBC mass can be detected accurately ~~from~~ for most particle types (e.g., Slowik et al., 2007; Cross et al., 2010), while determining the size of the particle containing both rBC and non-refractory material requires significant assumptions about the particle properties (e.g., Taylor et al., 2015). These uncertainties dealing with determining the particle sizes are further reflected in calculations
15 of mixing state parameters such as the rBC volume fraction in ~~absorbing particles each particle~~ and the number fraction of ~~absorbing rBC-containing~~ particles.

Due to the significant local and regional emissions and prevailing meteorological conditions, northern India is one of the global absorbing aerosol hot spots (Ramanathan et al., 2007). The low frequency of rainfall during the winter and spring months allows the accumulation of aerosol pollutions, which can be observed as a brown cloud (Ramanathan et al., 2001,
20 2007). Although the absorbing dust aerosol is mainly from natural origin, anthropogenic emissions such as ~~biomass-biofuel~~ burning and road traffic produce large amounts of black carbon. Aerosol concentrations are decreased significantly when the monsoon rains arrive (typically between mid-June and July in northern India). However, it has been suspected that the increased aerosol absorption could have an effect on the monsoon (e.g., Menon et al., 2002; Bollasina et al., 2008, 2011; Gautam et al., 2009; Lau et al., 2010; Ganguly et al., 2012; D'Errico et al., 2015; Boos and Storelvmo, 2016), which has a great importance
25 for the whole south Asia ~~region~~. In spite of the potential importance of the absorbing aerosol, there has been little published information about the BC mixing state in India.

The main purpose of this study is to provide new and detailed information about the rBC mixing state in northern India focusing on two different environments: polluted Indo-Gangetic plains and relatively clean Himalayan foothills. Comparing ~~these~~ observations gives us additional experimental information about processes affecting on the transport and uplift of absorbing
30 aerosol from the plains towards Himalayan foothills. Observations are made with a new measurement system where Differential Mobility ~~Particle Sizer (DMPS)~~ Analyzer (DMA) is used to size-select ambient particles before measuring rBC properties with a Single Particle Soot Photometer (SP2). This system provides ~~truly~~ size-resolved information about rBC mixing state parameters including rBC number fractions and rBC ~~volume in each absorbing mass in each~~ particle. Also, comparing the ~~DMPS-selected-DMA-selected~~ particle size with that ~~from measured by~~ the SP2 ~~measurements~~ gives additional information
35 about particle morphology.

2 Methods

2.1 Measurement sites

Mixing state of the rBC aerosol was measured in northern India in Mukteshwar, Nainital (29.47° N, 79.65° E, 2180 m above sea level) and Gual Pahari, Gurgaon (28.43° N, 77.15° E, 243 m above sea level) during the spring and pre-monsoon season 2014. Figure 1 shows the station locations. The measurements were started in Mukteshwar (9.2.-31.3.2014) and then the instruments were moved to Gual Pahari (3.4.-14.5.2014). Mukteshwar is a relatively clean site at the foothills of the central Himalayas about 2 km above the Indo-Gangetic plains (IGP) and Gual Pahari station is located at the plains close to Delhi where aerosol concentrations are significantly higher (e.g., Hyvärinen et al., 2009, 2010; Komppula et al., 2009; Panwar et al., 2013; Raatikainen et al., 2014; Hooda et al., 2016).

2.1.1 Measurement setup

Refractory black carbon (rBC) concentrations and mixing state parameters were measured by a Single Particle Soot Photometer (SP2; Revision C* with 8 channels), manufactured by the Droplet Measurement Technologies (Boulder, CO, USA), which was connected to a Differential Mobility Particle Sizer (DMPS). Details of the DMPS-SP2 measurement setup, data analysis and a series of consistency tests are given in the Supplementary Material. Briefly, the DMPS is composed of a ~~differential-mobility analyzer~~ Differential Mobility Analyzer (DMA) and a Condensation Particle Counter (CPC). The DMA selects narrow particle mobility size ranges from ~~dried (RH≈25 %)~~ polydisperse ambient particles (~~sampled through PM10 inlet line~~) and the CPC measures their number concentrations. Particle number concentrations are recorded for 30 logarithmically spaced mobility diameters (from about 20 to 650 nm) during a 32 minute scan (60 s in each mobility diameter and 120 s between scans). The actual ambient particle number size distribution is then inverted from the ~~sequential-CPC~~ observations by the user defined routines (Wiedensohler et al., 2012). The ~~inversion routines account mainly for the effects of the DMA transfer function and particle charging efficiencies including multiply charged particles.~~

The SP2 (see e.g., Stephens et al., 2003; Schwarz et al., 2006; Moteki and Kondo, 2007) was connected in parallel to the CPC ~~where it measures the number concentrations and sizes of both non-absorbing particles and those containing refractory absorbing material (Stephens et al., 2003; Schwarz et al., 2006; Moteki and Kondo, 2007). Although mineral dust and certain metal particles are refractory and absorbing,~~ to the outlet of the DMA. The SP2 measures number concentrations of particles with and without rBC for each mobility diameter. Any particle can be identified from the scattered laser light while only the rBC-containing particles emit visible light (incandescence). It is expected that the incandescence is originating from rBC, because clear evidence of ~~their contribution~~ other refractory species such as mineral dust was not observed (e.g. varying ratios between wide and narrow band incandescence signals) ~~were not observed. Therefore, all refractory material is considered to be refractory black carbon (rBC). In practice, the SP2 measures rBC mass.~~ Scattering and incandescence signal peak heights are proportional to the particle scattering cross section and rBC mass, respectively. The measured single particle rBC masses (0.3–380 fg) ~~from individual particles and this can be converted to a quantification range~~ were converted to rBC volume equivalent ~~diameter (70–740 nm when rBC is represented by a compact spherical core with diameters~~ (briefly just rBC core

diameter) by using 1800 kg m^{-3} density). ~~The rBC volume equivalent diameter (briefly rBC core diameter) is a commonly used parameter, but (70–740 nm diameter range).~~ These diameters are used even when it is well known that the ambient rBC is not necessarily spherical or compact (e.g., Bond and Bergstrom, 2006; Peng et al., 2016). ~~All number and mass concentrations measured by-~~ Number and volume mean rBC core diameters, average rBC mass concentration, and average number concentration of particles with and without rBC were calculated from the single particle data for each mobility diameter. In addition, the number fraction of particles containing rBC was calculated from the number concentrations of particles with and without rBC. Number (with and without rBC) and rBC mass size distributions were calculated from the corresponding mobility bin average number and mass concentrations using an applied inversion method. The DMPS inversion method is not directly suitable for SP2 data, because noise from mobility size bins close to the SP2 ~~were converted to actual size distributions by using~~ ~~the average DMPS inversion~~ (detection limit would have propagated to the relevant size bins. Therefore, we used the DMPS inversion results (number size distributions calculated from the CPC concentrations) to calculate size-dependent scaling factors that convert SP2 concentrations to corresponding size distributions (see the Supplementary Material). ~~The other-~~ Briefly, the size and scan dependent scaling factor is the inverted size distribution divided by the original CPC concentrations, but we have calculated the mode of the scaling factor for each mobility size bin to reduce the variability and to make the SP2 ~~parameters such as the fraction of particles containing rBC and the average rBC core diameter, which are now obtained as a function of mobility size and time, do not require this inversion.~~ results less dependent on the availability of the CPC data. This correction accounts for the effects of the DMA transfer function and particle charging efficiencies including multiply charged particles based on a typical particle size distribution. Multiply charged particles have also a small effect on the number and volume mean rBC core diameters, but these have been ignored based on visual examination of the rBC core size distributions (see Sect. 3.2).

20

Current measurement setup has some similarities with those used by Zhang et al. (2016) ~~and Liu et al. (2013)~~, Liu et al. (2013) and McMeeking et al. (2011), who coupled a SP2 with a Volatility Tandem Differential Mobility Analyzer (VTDMA) and Hygroscopicity Tandem Differential Mobility Analyzer (HTDMA). The VTDMA measures particle size distributions after exposing size-selected (200, 250, 300 and 350 nm) particles to $300 \text{ }^{\circ}\text{C}$ temperature (Zhang et al., 2016). The same size-selected particles are also measured by the SP2 allowing comparison between rBC core size distributions and those measured by the VTDMA. In the HTDMA-SP2 setup used by McMeeking et al. (2011) and Liu et al. (2013), size-selected particles (147, 193 and 286 nm in the first study and 163 and 259 nm in the second study) are exposed to a high RH ($\sim 90 \%$) and then measured by the SP2. There are also studies where the SP2 has been placed behind different types of classifiers such as the Aerosol Particle Mass (APM) analyzer or the Centrifugal Particle Mass Analyzer (CPMA) (e.g., Ohata et al., 2016). The main advantages of the current DMPS-SP2 setup is that the mobility size resolution is better (30 logarithmic size bins from about 20 nm to 650 nm) and ~~this allows the calculation of rBC mass and number size distributions~~ ~~can be determined~~.

Consistency tests showed that the SP2 over counted particles compared with the parallel CPC measurements (Supplementary Material). Multiplying all SP2 concentrations by a factor of 0.82 made the SP2 and CPC number concentrations levels similar with just noise-like variability. Consistency tests also showed that the DMA-selected mobility sizes are in good agreement with ~~the non-absorbing particle sizes those~~ measured by the SP2 (particles without rBC) although a weak dependency on the SP2

35

temperature was observed. ~~The last consistency test included a comparison~~ Comparison between rBC mass concentration with the optically detected (Aethalometer) equivalent BC (eBC) mass concentration from Mukteshwar. ~~Previous studies have shown that the rBC and eBC values can be different (e.g., Raatikainen et al., 2015), but the current values are within measurement uncertainties.~~ showed a strong correlation between mass concentrations (absolute values are not directly comparable) and that their ratio was independent of the SP2 temperature. Finally, laser power analysis showed that the average scattering signal was 93 % and 41 % from the original calibration value at Mukteshwar and Gual Pahari, respectively. Especially the latter drop in scattering signal could indicate critical drop in laser power. However, additional calculations showed that the reduced laser power is high enough for detecting rBC from particles with mobility sizes above 200 nm. These consistency tests show that the instrument setup and the data analysis methods provide accurate size-resolved rBC size distributions and mixing state parameters.

3 Results

Any SP2 can measure rBC core mass distributions (i.e. rBC mass concentration as a function of rBC core volume equivalent diameter) with high time resolution, however, the current size-selected measurements give this information for each DMA-selected mobility ~~partiele size~~ diameter. Knowing the particle (mobility) size simplifies the calculations especially for ~~absorbing~~ rBC-containing particles, which evaporate when travelling through the laser beam. For those particles, Leading Edge Only (LEO) methods (e.g., Gao et al., 2007; Metcalf et al., 2012; Laborde et al., 2012) can be used to calculate the optical size from the scattered laser light, but the calculations require additional particle position information and the results depend on the assumed particle structure and optical parameters. In the following calculations particle size is ~~assumed to be represented by~~ the DMA-selected mobility diameter, ~~which is the case for spherical particles~~. However, optical and mobility sizes are compared in Sect. 3.6 to obtain additional information about particle morphology.

~~Thanks to the significantly improved size resolution, it is possible to examine how much variability is there within each DMA-selected particle size.~~ Size-selected measurements allow the detailed examination of the rBC homogeneity, i.e. the variability of the rBC core size within each mobility size bin (Sect. 3.2). ~~It is often assumed that each particle size has a narrow unimodal distribution of rBC core sizes, but we show that this is not always the case.~~ Since this level of detail is ~~rarely not~~ typically needed, we will focus on the particle properties averaged for each DMA-selected ~~size.~~ This means that we calculated mobility size bin. These values are used to calculate rBC number and mass size distributions and size-dependent rBC mixing state parameters (number fraction of particles containing rBC and the average ~~volume fractions of rBC and non-refractory material in absorbing particles~~). ~~These size distribution and mixing state parameters have also variations in time.~~ rBC core size in those particles) for each size scan. Their average values are described in Sects 3.3 and 3.4 and diurnal cycles in Sect. 3.5. First, we give an overview of the measured parameters and their time variations using the total rBC mass concentration as an example (Sect. 3.1).

3.1 Total rBC mass concentration time series

As an example of the measured parameters and their time variations, the total rBC mass concentration time series from the ~~both measurement stations~~ site at the polluted Indo-Gangetic plains (Gual Pahari) and the relatively clean site at the Himalayan foothills (Mukteshwar) are shown in Fig. 2. Time series of the other parameters, which will be described below, are shown in the Supplementary Material. The average rBC mass concentrations and their standard deviations are 11 ± 11 and $1.0 \pm 0.6 \mu\text{g m}^{-3}$ for Gual Pahari and Mukteshwar, respectively. Figure 2 shows that the rBC mass concentrations are highly variable, which is the reason for the high standard deviations (absolute measurement uncertainties are close to 20 % (e.g., Laborde et al., 2012)), and the variability is dominated by their diurnal cycles. Statistically significant long term trends or weekly cycles cannot be found. Detailed examination of the diurnal variations of the total rBC mass and the other measured rBC mixing state parameters will be given in Sect. 3.5. ~~Figure 2 also shows the clear difference in rBC mass concentration between the site at the polluted Indo-Gangetic plains (Gual Pahari) and the relatively clean site at the Himalayan foothills (Mukteshwar). These differences will be examined in the following sections.~~

3.2 Size-selected rBC homogeneity

~~Size-selected measurements of~~ Examining size-selected rBC core size distributions can show how homogeneous ~~absorbing~~ these rBC-containing particles are. ~~When a sufficiently large mobility size (≥ 200 nm) is selected, multiple rBC core diameter modes appear especially in Mukteshwar~~ The selected mobility size must be large enough so that the thickly coated rBC can be detected, but still small enough to represent the accumulation mode particles. Examination of the available mobility sizes showed that the 360 nm mobility diameter is optimal for this purpose (the limits are shown in the Supplementary Material). Figure 3 shows the campaign average rBC core number size distributions from particles with 360 nm DMA-selected mobility diameter. ~~This mobility size seem to be optimal for most calculations as it is representative of the accumulation mode and has enough particles for good counting statistics; although the standard deviations for the concentration-dependent parameters such as the average rBC core number size distributions (standard deviation not shown in Fig. 3) are comparable with the corresponding average values, these are mainly caused by the clear diurnal concentration variations seen in Fig. 2. The 360 nm mobility size is also large enough to avoid missing the rBC cores from “thickly coated” particles (about 70 nm detection limit for rBC volume equivalent diameter). This is the reason why current calculations are limited to mobility sizes larger than ~ 200 nm.~~

(variability shown in the Supplementary Material). When Gual Pahari rBC core size distribution is mostly unimodal (mode at about 180 nm), that at Mukteshwar is clearly bimodal where the smaller mode is located at about 110 nm and the other dominating mode is at about 210 nm. Changing the DMA-selected diameter to a larger or smaller value does not reveal any additional modes. ~~It should be noted that here the particles larger than about 300 nm are most likely from~~ and the same larger mode is always dominating. The modes are relatively wide mainly due to the width of DMA transfer function (the full width at half maximum is about 45 nm for the 360 nm mobility size). The tails of the size distributions are related to the instrument noise (below 85 nm and above 300 nm) and multiply charged particles (~~no clear evidence of pure compact rBC; see Sect. 3.6~~ above

300 nm), but ~~their contributions for the rBC core mean diameter and the total particle number and mass are negligible. they~~ have small contributions to the mobility size bin mean values that are used in the following sections (86 % and 92 % of the particles between 85 and 300 nm in Gual Pahari and Mukteshwar, respectively). In general, the modes at about 200 nm seem to be quite similar for Gual Pahari and Mukteshwar while the smaller mode at about 110 nm is clearly seen only at Mukteshwar.

5 Figure 3 shows the campaign average core size distributions for the 360 nm mobility diameter, but we have also calculated those for each size scan. Mukteshwar rBC core number size distribution seems to be bimodal most of the time. The number fraction of the larger rBC particles (those larger than 140 nm from the 85–300 nm core size range) varies between 0.5 and 0.8. The fluctuations are irregular covering several days, and mainly for this reason, there are no significant diurnal variations (not shown). ~~The lack of diurnal variations indicates that the mixing of local and long-range transported (from the Indo-Gangetic~~
10 ~~plains or aloft) air masses is not the main reason for the bimodal rBC size distribution (this explains the diurnally varying rBC mass concentration described in Sect. 3.5). Another explanation for the observed bimodal rBC distribution is that the smaller and larger particles are originating from different local sources.~~

3.3 Average rBC size distributions

Since rBC homogeneity within a DMA-selected mobility size bin is too detailed information for most practical applications,
15 ~~the following calculations are based on rBC properties averaged over each DMA-selected mobility size . Because rBC core size distributions are not fully unimodal, the average rBC core diameter is calculated based on both particle number (as in Fig. 3) and mass (or volume, which is just the rBC mass divided by the constant density of 1800). The former is simply the number average rBC core diameter and the latter is representative of the rBC core mean mass so that the correct total rBC mass can be obtained by multiplying the core mean mass by the total number of particles containing rBC. The number fraction of particles~~
20 ~~containing rBC, $N_{\text{rBC}}/N_{\text{total}}$, is also calculated for each DMA-selected mobility size by using the total number of observed particles and that for particles containing rBC. Finally, logarithmic rBC number and mass size distributions are calculated (see the Supplementary Material) and described with the total number and mass concentration and geometric (mass) mean diameter and standard deviation. for each mobility size bin in each scan.~~

3.3 Average rBC size distributions

25 Figure 4 shows the campaign average rBC core mass and number size distributions from the both measurement sites ~~during the campaign period. The dip~~. The gap at about 300 nm is caused by ~~a gap between discontinuous~~ high and low gain rBC mass calibration parameterizations. Due to the significant diurnal variations, which will be discussed later, the average mass and number size distributions have standard deviations (not shown) that are proportional to the observed size bin mean values. It is evident from Fig. 4 that the number size distributions are not fully resolved due to the about 70 nm rBC core size detection
30 limit. Therefore, we will focus on the rBC mass size distributions. These have similar shapes except that the concentrations at Gual Pahari are about ten times higher than those at Mukteshwar. Both mass distributions peak at around 210 nm, but these have relatively high concentrations of larger particles especially at Gual Pahari. Large particles are also observed in the number and mass size distributions measured by the DMPS (shown in the Supplementary Material). ~~The large absorbing refractory~~

~~particles are most likely rBC~~ Bimodal log-normal distributions fitted to the mass distributions are shown with three (both modes and the total) thin blue (Mukteshwar) and green (Gual Pahari) lines in Fig. 4. The fits show that the peak diameters of the main modes are 195 and 202 nm and the main modes cover 76 % and 93 % of the observed rBC mass in Gual Pahari and Mukteshwar, respectively. Because only the tails of the modes with larger particles are seen (their peak diameters are larger than the rBC core detection limit, 740 nm), it is not possible to quantify their contributions to the total rBC mass. ~~Dust particles and rBC have different boiling points, which would mean different wide band to narrow band incandescence ratios (Moteki and Kondo, 2007), but such changes were not seen.~~

Figure 4 shows the campaign average distributions, but we have also calculated ~~the corresponding time series (rBC mass concentrations time series is shown in Fig. 2 and the other times series are shown in the Supplementary Material).~~ These ~~log-normal mass distributions~~ those for each mobility scan. Although the mass distributions are somewhat skewed, these can be described ~~by the~~ relatively well by log-normal distributions. We have therefore calculated the time series of total rBC mass concentrations ~~and the~~ (shown in Fig. 2) and geometric mass mean ~~diameter and standard deviation. Average diameters and standard deviations~~ (shown in the Supplementary Material). The average size distribution parameters and their standard deviations from both measurement sites are shown in Table 1. The diurnal variations of the key rBC size distribution and mixing state parameters are ~~also~~ shown in Sect. 3.5.

~~The observed total rBC mass concentrations are similar to the typical optically measured equivalent BC (eBC) concentrations. For example, previous long term measurements have shown that the average April and May eBC concentrations in Gual Pahari are 8.5 and 5.7 (Hooda et al., 2016), respectively, and those in Mukteshwar are 1.4 and 1.2 (Hyvärinen et al., 2009). Since our simultaneous SP2 and Aethalometer measurements from Mukteshwar show good agreement between rBC and eBC concentrations (shown in the Supplementary Material), current measurements seem to represent typical pre-monsoon season conditions.~~

Previous SP2 studies have reported rBC core size distribution parameters from various environments (e.g. summary in Huang et al., 2012), but to our knowledge there are no previously published results from India. However, equally high rBC concentrations are observed in China and there SP2 studies have shown that rBC core peak diameters are close to 220 nm ~~(Huang et al., 2011, 2012)~~ (Huang et al., 2011, 2012; Wang et al., 2014), which are in good agreement with the current observations (peaks at about 210 nm). ~~Due to the presence of large~~ Huang et al. (2011) and Wang et al. (2014) have also observed bimodal rBC size distributions, but the larger particles (>400 nm) ~~rBC cores, geometric mean diameter is somewhat higher in Gual Pahari than in Mukteshwar or in these previous observations elsewhere~~ have significantly higher contribution in India. In general, mass mean diameters are relatively similar at least compared with concentrations which vary by several orders of magnitude depending heavily on local ~~and regional~~ emission sources.

3.4 Average rBC mixing state

Mixing state can be described by two ~~size-dependent~~ parameters that are directly measured by the ~~DMPS-SP2 system~~ SP2: number fraction of particles containing rBC ($N_{\text{rBC}}/N_{\text{total}}$) and rBC ~~volume fraction mass~~ in these particles. ~~For simplicity, it is expected that particles are spherical so that their volumes can be calculated using the mobility diameter (some indirect evidence~~

about the actual particle morphology is given in Sect. 3.6). With this assumption rBC volume fraction is proportional to the rBC core to mobility diameter ratio. Because rBC core diameters show, which is here represented by the rBC core diameter (volume equivalent diameter based on 1800 kg m^{-3} rBC density). Because core diameters showed some variability (Fig. 3), we have calculated both number and volume mean rBC core diameters ($D_{\text{rBC},N}$ and $D_{\text{rBC},V}$) and. We also present their ratios with the mobility diameters (D_m). Since these particles may not be spherical (some indirect evidence is given in Sect. 3.6), rBC core to mobility diameter ratios should not be taken as an exact measure of the rBC volume fraction. These parameters depend on mobility size and time, but the time series are correlated. Therefore, conclusions can be made using only one time series and mean values for each mobility size. Again, we use the 360 nm mobility size to represent the typical accumulation mode particles.

10 The campaign average mixing state parameters and their standard deviations for the 360 nm mobility size are shown in Table 1. ~~Their diurnal variations are examined in Sect. 3.5.~~

~~The data in Table 1 shows that a relatively large fraction of particles contain detectable amounts of rBC, but these absorbing particles have low rBC volume fractions in both Gual Pahari and Mukteshwar.~~ As expected, the rBC number fraction is somewhat larger in Gual Pahari (polluted region) than in Mukteshwar (regional background), but the absorbing rBC-containing particles seem to have similar rBC volume fraction core diameters. It could have been expected that rBC volume fraction decreases when semi-volatile core size decreases when secondary aerosol species such as organics and sulfate condense to existing particles during their transport to Mukteshwar, but this effect is not clearly seen, although it may contribute to the observed bimodal rBC core size distribution seen in Fig. 3. It seems that the observed rBC properties are common for the whole region due to the similar emission sources and relatively short times for aging (more likely hours than days). For example, air masses in the upper troposphere or in remote regions can have spent several days without any contact to rBC sources.

There are some previous studies that describe the rBC mixing state with this level of details. It is evident that most particles do not contain detectable amounts of rBC anywhere (e.g., Kondo et al., 2011; Reddington et al., 2013; Dahlkötter et al., 2014; Raatikainen et al., 2015), but the current number fractions of rBC-containing particles (46 % and 31 % for the 360 nm mobility size at Gual Pahari and Mukteshwar, respectively) seem to be the highest so far. For example, our previous results from the Finnish Arctic show that 24 % of the particles from 350–450 nm optical diameter range contain rBC and this is already a relatively large fraction (Raatikainen et al., 2015). In India, the high number fraction of rBC-containing particles is probably resulting in resulting from the significant local and regional biomass burning regional black carbon emissions. The observed rBC core to particle diameter ratios ($D_{\text{rBC},V}/D_m$ or ~ 0.6 and $D_{\text{rBC},N}/D_m \sim 0.5$ from Table 1), which represent rBC volume fractions, are quite low for a fresh aerosol anywhere cube is rBC volume fraction in a spherical compact particle, are larger than those observed for aged aerosol (e.g., Raatikainen et al., 2015; Dahlkötter et al., 2014), but match with the lowest values found for fresh emissions (e.g., Kondo et al., 2011; Schwarz et al., 2008; Sahu et al., 2012; Metcalf et al., 2012). Our qualitative analysis of particle morphology (see Sect. 3.6) indicates that the absorbing particles are fractal aggregates, which means that the mobility size is significantly larger than the actual volume equivalent diameter, but for the time being mobility size is used as a representative of the particle size. For example, Metcalf et al. (2012) found thickly coated rBC from an urban plume with rBC core to particle diameter ratios ranging from about 0.51 to 0.59 (145 nm rBC cores with 50–70 nm coating thicknesses).

Although the agreement is good, it should be noted that our particle size is based on the mobility diameter while most other studies use the optical diameter from the LEO method. We will show later (Sect. 3.6) that mobility sizes are larger than optical sizes, which means that our rBC core to particle (optical) diameter ratios actually represent fresh emissions.

Mixing state parameters are somewhat size-dependent and this can be parameterized using the size-selected measurements. Fig. 5 shows the averaged size dependent mixing state parameters (number and volume based rBC core diameters and number fractions of particles containing rBC) and simple parameterizations. The lowest particle sizes where the SP2 detection limit has a significant effect on the results have been excluded from the fits (indicated by the smaller marker below ~ 200 nm particle size). Also, the largest particle size in Mukteshwar has also been excluded due to the low number of observed particles. In general, the trends in the rBC mixing state parameters are similar for Gual Pahari and Mukteshwar, which indicates fairly similar local and regional rBC sources.

3.5 Diurnal cycles

Figure 6 shows the diurnal cycles of the rBC mass distribution (total mass and geometric mass mean diameter and standard deviation) and mixing state (rBC core to **particle-mobility** diameter ratio and the number fraction of particles containing rBC for the 360 nm mobility size bin) parameters. The number based diameter ratios and size distribution parameters are not shown, because these have similar diurnal variations with the mass and volume based parameters. The total rBC mass concentrations have significant diurnal variations while those for the mean diameter and distribution width are modest. From the rBC mixing state parameters, which are not directly related to the mass distribution, only the rBC particle number fractions have clear diurnal cycles while the rBC core to **particle-mobility** diameter ratio is practically constant.

~~Strong~~ The strong diurnal variability of the ~~optically measured~~ rBC mass concentrations is in good agreement with those of equivalent black carbon and the total particulate mass in general have been observed in our previous studies and by others (e.g., Komppula et al., 2009; Hyvärinen et al., 2009, 2010; Panwar et al., 2013; Raatikainen et al., 2014); and similar diurnal cycles are also seen in the rBC mass concentrations. Aerosol pollutions from local and regional sources accumulate to the shallow boundary layer during late evening and night at the Indo-Gangetic plains (represented by Gual Pahari). At this time rBC number fractions are also the highest. Aerosol concentrations and rBC number fractions decrease in the morning due to the increased vertical mixing. During the pre-monsoon season, when boundary layer heights typically exceed 2000 m, polluted air masses from Indo-Gangetic plains reach the altitude of Mukteshwar station during afternoons (Raatikainen et al., 2014). This is seen as a significant increase in total aerosol and rBC concentrations, but the other rBC parameters are practically unchanged. This means that transported aerosols have already become similar to the background aerosols, i.e. lost a fraction of the largest absorbing particles and grown by condensation of a non-refractory material. Increased vertical mixing is the main reason for the daytime decrease in rBC mass in Gual Pahari and this can also explain the decrease in rBC number fraction. In general, ~~fresh (Gual Pahari) and background (Mukteshwar)~~ Gual Pahari and Mukteshwar rBC aerosols are relatively similar except that the ~~fresh~~ Gual Pahari aerosol has an order of magnitude higher concentration and the number fraction of particles containing rBC is about 50 % larger compared with those from ~~the background site~~ Mukteshwar.

3.6 Morphology of **absorbing-rBC-containing** particles

Black carbon or soot particles are initially aggregates composed of several primary BC particles, which diameters are in the order of a few tens of nanometers (e.g., Sorensen, 2001). These fresh aggregates can contain some amounts of a non-refractory material, but the fraction increases with time when atmospheric vapours condense to the soot particles and when the particle ~~grew~~ grows by coagulation. Increasing non-refractory fraction makes these particles more spherical. In addition, aggregates can be compacted when particles absorb water vapour and become droplets (e.g., Zhang et al., 2008; Pagels et al., 2009). As a result, core-shell structure can be a valid approximation for the aged aerosol, but it is not clear if this is the case in India, where the aerosol is relatively fresh. The SP2 can provide some information about the morphology of the **absorbing-rBC-containing** particles.

10 First, the SP2 can detect if a particle disintegrates in the laser beam into rBC and **non-absorbing-non-rBC** fragments. This can happen if the rBC core is close to the particle surface or when rBC is attached to the surface of another particle (Sedlacek et al., 2012; Moteki et al., 2014). However, ~~current experiments showed our~~ measurements show that such disintegrating particles have negligible concentrations.

There are also studies reporting bare rBC particles (e.g., Huang et al., 2012), but the current rBC core volume equivalent 15 diameters are always well below mobility diameters. However, it is possible that the rBC particles have low densities or that the particles are irregular aggregates. At least qualitative information about the particle shape can be obtained by comparing the DMA-selected mobility and SP2-derived optical sizes. Optical size is based on the measured or reconstructed (see below) intensity of the scattered laser light and a theoretical correction to the scattering accounting for the difference between calibration (ammonium sulfate) and ambient aerosol structures and optical properties. Accurate sizing requires information about particle 20 structure, but clear differences (e.g. **much larger than the typical $\pm 20\%$ sizing uncertainty**) between optical and mobility sizes (**at least $\pm 10\%$**) indicate non-spherical particles such as aggregates.

3.6.1 **Optical size based on a LEO method**

Optical sizes are estimated using Leading Edge Only (LEO) methods (e.g., Gao et al., 2007; Metcalf et al., 2012; Laborde et al., 2012). In earlier studies, the authors use the leading edge of the scattering signal, which is yet unaffected by the evaporation 25 of the non-refractory material, to reconstruct the unperturbed scattering signal. Current method is the same as the method used in our previous study (Raatikainen et al., 2015): here the leading edge is the part of the signal where laser beam intensity is 0.07–3 % of the maximum, and the Gaussian scattering (laser beam) profile and peak position are calculated by averaging those from 100 previous ~~non-absorbing particles~~. **Signal particles that do not have detectable incandescence signal. Scattering signal peak height is solved by fitting the Gaussian profile to the signal from the leading edge (e.g., Gao et al., 2007). Although the** 30 **Scattering cross section is calculated from the signal peak height by using the scattering calibration, and optical particle size is calculated from the scattering cross section by using the Mie theory (linear interpolation between the limits of pure ammonium sulfate (refractive index $m=1.48-i0$) and a mixed particle ($m=1.715-i0.395$) with rBC core to particle diameter ratio of 0.6).**

The current LEO analysis suffered from a ~~noise signal~~-systematic noise signal, which increased the variability of the results and seemed to cause a systematic bias when the instrument temperature was below 30 °C (see the Supplementary Material); ~~which reduces the reliability of the results, the difference between the DMA-selected mobility and optical size is clear. Taking~~. Also, the decrease in laser power when the SP2 was transported from Mukteshwar to Gual Pahari decreased the success rate of the LEO fits from 98.6 % to 90.9 % (for rBC-containing particles from the 360 nm mobility size bin). Due to these uncertainties, we focus on the 360 nm mobility size bin ~~as an example, the average LEO-calculated optical size for absorbing particles is only about 220 nm in both~~ and use data from instrument temperatures between 30 and 35 °C. These results seem to be reliable, but potential biases cannot be fully ruled out.

For the 360 nm mobility size and when the instrument temperature is between 30 and 35 °C, the campaign average LEO-derived optical particle diameters for rBC-containing particles are 245 ± 10 and 234 ± 20 nm for Mukteshwar and Gual Pahari ~~(non-absorbing particles have almost equal LEO-calculated optical and mobility sizes). This 220 nm~~, respectively. For reference, corresponding sizes for particles without rBC are 360 ± 25 and 359 ± 17 nm, which are in good agreement with those without the LEO method (356 ± 7 and 361 ± 11 nm) and the selected mobility diameter (360 nm). It is clear that the average optical size is ~~quite close to the mean rBC core volume equivalent diameter (Table 1: approx. 180 nm for the 360 nm DMA size), which is indicative of scattering from~~ significantly smaller than the mobility size, which shows that the rBC-containing particles are not spherical. Further examination of the single particle data can reveal additional details about individual particles. Figure 7 shows the dependency of the optical size on the rBC core size by means of a probability density map (darker color means higher probability). The rBC core size population is clearly bimodal in Mukteshwar (see Sect. 3.2) and it seems that the smaller rBC cores are thickly coated (core to optical diameter ratio approx. 0.4) while the larger rBC cores are thinly coated (core to optical diameter ratio close to unity). The only clear rBC mode in Gual Pahari seems to be thinly coated. The red markers and error bars show the effect of refractive index on the calculated optical size; the upper limit is based on ammonium sulfate refractive index ($m=1.48-i0$) and the lower limit is based on that of pure rBC ($m=2.26-i1.26$ from Moteki et al. (2010)). Additional uncertainties arise from the particle morphology (e.g. He et al., 2015) and scattering model (e.g. He et al., 2016). Even when considering these large potential uncertainties, the optical sizes are smaller than the mobility sizes, which show that rBC-containing particles are not spherical. Especially the thinly coated particles are most likely highly fractal soot aggregates. Such aggregates typically have low volume fractions of non-refractory material, but the exact fractions cannot be determined without detailed information about particle morphology and optical properties (e.g. He et al., 2016).

Zhang et al. (2016) used similar measurement setup (VTDMA-SP2) in northern China about 60 km from Beijing. They have found closely matching LEO-calculated optical and mobility sizes, which indicates spherical particle shape, and internally mixed particles with low rBC volume fraction (161 nm mass equivalent rBC core size for 350 nm mobility size). Although the rBC concentrations have similar magnitudes in northern China and India, ~~absorbing rBC-containing~~ particles seem to have different properties most likely due to different sources.

~~Additional information about aggregate properties can be found by calculating parameters such as effective densities, dynamic shape factors and mass fractal dimensions, which are based on the measured particle mass and mobility diameter (e.g., Zhang et al., 2008; Pagels et al., 2009; Peng et al., 2016). The SP2 can detect the total rBC mass from each particle~~

(e.g., Slowik et al., 2007), but non-refractory mass cannot be determined from irregular particles. Therefore, we will focus on the mass fractal dimension parameter, which can be less sensitive on the possibly missing non-refractory mass. Empirical equations of the same kind have been often used in cases where particle mass (m) and mobility size (D_m) are known while the structural details are missing (e.g., Zhang et al., 2008; Pagels et al., 2009):-

$$m = AD_m^{Dfm}$$

Here Dfm is the mass fractal dimension and it is a fitting parameter in addition to the constant A . Constant A depends directly on the absolute particle mass while Dfm is independent of that when the possibly missing non-refractory mass is a constant fraction of the observed mass. Dfm is indicative of the compactness of the particle: values close to 3 mean a sphere and lower values indicate less ideal particle shape. Figure ?? shows the average rBC mass (calculated from the mass mean core volume equivalent diameter) as a function of mobility diameter and a fit (initially log-log scale: $\log(m) = \log(A) + Dfm \log(D_m)$) to the data for both Mukteshwar and Gual Pahari. Both Gual Pahari and Mukteshwar mass fractal dimensions are low (1.72 and 1.85, respectively) indicating highly fractal particle structure (e.g., Pagels et al., 2009). This is in a qualitative agreement with the findings of ? who observed the dominance of freshly formed soot particles with an open branched structure in Sinhadgad near Pune in western India during April 2006.-

Mass fractal dimensions were also found for individual measurements using the same fitting method (not shown). The Dfm time series show larger and more irregular variations in Mukteshwar (the 10th and 90th percentiles are 1.38 and 2.22, respectively) than in Gual Pahari (the 10th and 90th percentiles are 1.48 and 1.95, respectively). As a result, there are no clear diurnal cycles in Mukteshwar where hourly averages (\pm standard deviation) range from 1.76 ± 0.29 at 17:00-18:00 LT to 2.00 ± 0.35 at 05:00-06:00 LT. The hourly averages in Gual Pahari range from 1.61 ± 0.15 at 04:00-05:00 LT to 1.90 ± 0.20 at 15:00-16:00 LT, which means small but observable diurnal cycle. Nevertheless, the highly fractal particles with Dfm less than two seem to be dominating at least in Gual Pahari. This indicates slower aging than in Mexico City, where photochemical activity results in rapid conversion of fresh soot to spherical coated soot (?)-

4 Conclusions

Refractory black carbon (rBC) mass distributions and mixing state parameters were measured using a size-selected Single Particle Soot Photometer (SP2) in northern India during spring 2014. The size-selected results were obtained by connecting a SP2 to the outlet of a Differential Mobility Analyzer (DMA), which classifies particles according to their mobility size. The measurements were made in a relatively clean regional background site at the Himalayan foothills (Mukteshwar) and at a relatively polluted site close to Delhi (Gual Pahari). To our knowledge, this is the first publication showing size-selected rBC mass distributions and mixing state parameters for this region.

The measurements show that ~~about 30-50 %~~ $46 \pm 12 \%$ and $31 \pm 5 \%$ of the accumulation mode particles contain observable amounts of rBC in Gual Pahari and Mukteshwar, respectively. Just as the absolute rBC concentrations ~~;~~ (11 ± 11 and $1.0 \pm 0.6 \mu\text{g m}^{-3}$ in Gual Pahari and Mukteshwar, respectively), the rBC particle number fraction is higher at the source ~~regions~~ region

(represented by Gual Pahari) and lower at elevated altitudes (Mukteshwar). Although literature data about rBC mixing state is limited (e.g., Raatikainen et al., 2015; Dahlkötter et al., 2014; Reddington et al., 2013), the observed number fractions of particles containing rBC are the highest reported so far.

The observed rBC particles are likely to contain ~~a non-refractory material~~ materials such as sulfate and organics, but the exact volume fractions could not be quantified, ~~because these particles are not spherical~~. Current rBC volume equivalent to mobility diameter ratios (number mean $D_{rBC,N}/D_m \sim 0.5$ ~~for both measurements sites~~ are 0.51 ± 0.02 and 0.50 ± 0.03 for Gual Pahari and Mukteshwar, respectively) would mean that ~~such~~ spherical particles have lower rBC volume fractions than expected for fresh particles (e.g., Schwarz et al., 2008; Sahu et al., 2012). However, optical sizes determined using a Leading Edge Only (LEO) method were significantly smaller than the mobility diameters, which indicates that the rBC-containing particles are highly irregular such as fractal aggregates. The rBC diameter to optical size ~~ratio ratios~~ (~ 0.8 ~~for both measurement sites~~) ~~is at Gual Pahari and ~ 0.7 at Mukteshwar~~ are closer to value expected for fresh aerosol, but these calculations are also limited by the fact that the optical size is based on assumed optical parameters and spherical core-shell structure. ~~Furthermore, the clear difference between optical and mobility sizes as well as low values of fitted mass fractal dimensions (see e.g., Pagels et al., 2009) indicate that the rBC particles are most likely highly irregular fractal aggregates. In that case the exact calculations of particle size or total material volume are~~ The exact calculation of particle composition is not possible without additional details about particle structure.

Although individual particles seem to be quite similar in Gual Pahari and Mukteshwar, the total rBC concentrations are about ten times higher at the more polluted site, Gual Pahari, than those at the regional background site, Mukteshwar. Also, a larger fraction of the particles contain rBC in Gual Pahari than in Mukteshwar. One explanation for the similarity is that some aerosol sources are common for the whole region (e.g. ~~road traffic, biomass-crop residue and biofuel~~ burning and cooking). The other is that a significant fraction of the rBC seen in Mukteshwar can be originating from the densely populated Indo-Gangetic plains represented by Gual Pahari (Raatikainen et al., 2014).

Detailed information about the black carbon mixing state is needed for assessing and improving the performance of climate models in simulating their evolution and radiative effects. SP2 is one of the few instruments that can provide detailed information about the ~~absorbing aerosol~~ rBC mixing state. The accuracy of the mixing state parameters can be further improved by size-selecting the particles before measurements with the SP2; this method is especially suitable for polluted areas where good counting statistics is guaranteed.

Acknowledgements. Authors would like to acknowledge the Academy of Finland (project numbers 264242, 268004 and 284536), Academy of Finland Centre of Excellence Program (project number 272041) and KONE foundation for the financial support. We thank to local TERI staff for 24/7 work at Mukteshwar aerosol research station.

References

- Adachi, K., Chung, S. H., and Buseck, P. R.: Shapes of soot aerosol particles and implications for their effects on climate, *J. Geophys. Res.*, 115, D15 206, doi:10.1029/2009JD012868, 2010.
- Bollasina, M., Nigam, S., and Lau, K.-M.: Absorbing Aerosols and Summer Monsoon Evolution over South Asia: An Observational Portrait, *J. Clim.*, 21, 3221–3239, doi:10.1175/2007JCLI2094.1, 2008.
- Bollasina, M. A., Ming, Y., and Ramaswamy, V.: Anthropogenic Aerosols and the Weakening of the South Asian Summer Monsoon, *Science*, 334, 502–505, doi:10.1126/science.1204994, 2011.
- Bond, T. C. and Bergstrom, R. W.: Light Absorption by Carbonaceous Particles: An Investigative Review, *Aerosol Sci. Tech.*, 40, 27–67, doi:10.1080/02786820500421521, 2006.
- 10 Bond, T. C., Doherty, S. J., Fahey, D. W., Forster, P. M., Berntsen, T., DeAngelo, B. J., Flanner, M. G., Ghan, S., Kärcher, B., Koch, D., Kinne, S., Kondo, Y., Quinn, P. K., Sarofim, M. C., Schultz, M. G., Schulz, M., Venkataraman, C., Zhang, H., Zhang, S., Bellouin, N., Guttikunda, S. K., Hopke, P. K., Jacobson, M. Z., Kaiser, J. W., Klimont, Z., Lohmann, U., Schwarz, J. P., Shindell, D., Storelvmo, T., Warren, S. G., and Zender, C. S.: Bounding the role of black carbon in the climate system: A scientific assessment, *J. Geophys. Res.-Atmos.*, 118, 5380–5552, doi:10.1002/jgrd.50171, 2013.
- 15 Boos, W. R. and Storelvmo, T.: Near-linear response of mean monsoon strength to a broad range of radiative forcings, *P. Natl. Acad. Sci. USA*, 113, 1510–1515, doi:10.1073/pnas.1517143113, 2016.
- Cappa, C. D., Onasch, T. B., Massoli, P., Worsnop, D. R., Bates, T. S., Cross, E. S., Davidovits, P., Hakala, J., Hayden, K. L., Jobson, B. T., Kolesar, K. R., Lack, D. A., Lerner, B. M., Li, S.-M., Mellon, D., Nuaaman, I., Olfert, J. S., Petäjä, T., Quinn, P. K., Song, C., Subramanian, R., Williams, E. J., and Zaveri, R. A.: Radiative Absorption Enhancements Due to the Mixing State of Atmospheric Black Carbon, *Science*, 337, 1078–1081, doi:10.1126/science.1223447, 2012.
- ~~Coz, E. and Leck, C.: Morphology and state of mixture of atmospheric soot aggregates during the winter season over Southern Asia—a quantitative approach, *Tellus B*, 63, 107–116, 2011.~~
- 20 Cross, E. S., Onasch, T. B., Ahern, A., Wrobel, W., Slowik, J. G., Olfert, J., Lack, D. A., Massoli, P., Cappa, C. D., Schwarz, J. P., Spackman, J. R., Fahey, D. W., Sedlacek, A., Trimborn, A., Jayne, J. T., Freedman, A., Williams, L. R., Ng, N. L., Mazzoleni, C., Dubey, M., Brem, B., Kok, G., Subramanian, R., Freitag, S., Clarke, A., Thornhill, D., Marr, L. C., Kolb, C. E., Worsnop, D. R., and Davidovits, P.: Soot Particle Studies—Instrument Inter-Comparison—Project Overview, *Aerosol Sci. Tech.*, 44, 592–611, doi:10.1080/02786826.2010.482113, 2010.
- Dahlkötter, F., Gysel, M., Sauer, D., Minikin, A., Baumann, R., Seifert, P., Ansmann, A., Fromm, M., Voigt, C., and Weinzierl, B.: The Pagami Creek smoke plume after long-range transport to the upper troposphere over Europe – aerosol properties and black carbon mixing state, *Atmos. Chem. Phys.*, 14, 6111–6137, doi:10.5194/acp-14-6111-2014, 2014.
- 30 D’Errico, M., Cagnazzo, C., Fogli, P. G., Lau, W. K. M., von Hardenberg, J., Fierli, F., and Cherchi, A.: Indian monsoon and the elevated-heat-pump mechanism in a coupled aerosol-climate model, *J. Geophys. Res.-Atmos.*, 120, 8712–8723, doi:10.1002/2015JD023346, 2015.
- Ganguly, D., Rasch, P. J., Wang, H., and Yoon, J.-H.: Climate response of the South Asian monsoon system to anthropogenic aerosols, *J. Geophys. Res.-Atmos.*, 117, D13 209, doi:10.1029/2012JD017508, 2012.
- 35 Gao, R. S., Schwarz, J. P., Kelly, K. K., Fahey, D. W., Watts, L. A., Thompson, T. L., Spackman, J. R., Slowik, J. G., Cross, E. S., Han, J.-H., Davidovits, P., Onasch, T. B., and Worsnop, D. R.: A Novel Method for Estimating Light-Scattering Properties of Soot Aerosols Using a Modified Single-Particle Soot Photometer, *Aerosol Sci. Tech.*, 41, 125–135, doi:10.1080/02786820601118398, 2007.

- Gautam, R., Hsu, N. C., Lau, K.-M., and Kafatos, M.: Aerosol and rainfall variability over the Indian monsoon region: distributions, trends and coupling, *Ann. Geophys.*, 27, 3691–3703, doi:10.5194/angeo-27-3691-2009, 2009.
- He, C., Liou, K.-N., Takano, Y., Zhang, R., Levy Zamora, M., Yang, P., Li, Q., and Leung, L. R.: Variation of the radiative properties during black carbon aging: theoretical and experimental intercomparison, *Atmos. Chem. Phys.*, 15, 11 967–11 980, doi:10.5194/acp-15-11967-2015, 2015.
- He, C., Takano, Y., Liou, K.-N., Yang, P., Li, Q., and Mackowski, D. W.: Intercomparison of the GOS approach, superposition T-matrix method, and laboratory measurements for black carbon optical properties during aging, *J. Quant. Spectrosc. Ra.*, 184, 287–296, doi:10.1016/j.jqsrt.2016.08.004, 2016.
- Hooda, R., Hyvärinen, A.-P., Vestenius, M., Gilardoni, S., Sharma, V., Vignati, E., Kulmala, M., and Lihavainen, H.: Atmospheric aerosols local–regional discrimination for a semi-urban area in India, *Atmos. Res.*, 168, 13–23, doi:10.1016/j.atmosres.2015.08.014, 2016.
- Huang, X.-F., Gao, R. S., Schwarz, J. P., He, L.-Y., Fahey, D. W., Watts, L. A., McComiskey, A., Cooper, O. R., Sun, T.-L., Zeng, L.-W., Hu, M., and Zhang, Y.-H.: Black carbon measurements in the Pearl River Delta region of China, *J. Geophys. Res.-Atmos.*, 116, doi:10.1029/2010JD014933, 2011.
- Huang, X.-F., Sun, T.-L., Zeng, L.-W., Yu, G.-H., and Luan, S.-J.: Black carbon aerosol characterization in a coastal city in South China using a single particle soot photometer, *Atmos. Environ.*, 51, 21–28, doi:10.1016/j.atmosenv.2012.01.056, 2012.
- Hyvärinen, A.-P., Lihavainen, H., Komppula, M., Sharma, V. P., Kerminen, V.-M., Panwar, T. S., and Viisanen, Y.: Continuous measurements of optical properties of atmospheric aerosols in Mukteshwar, northern India, *J. Geophys. Res.*, 114, D08 207, doi:10.1029/2008JD011489, 2009.
- Hyvärinen, A.-P., Lihavainen, H., Komppula, M., Panwar, T. S., Sharma, V. P., Hooda, R. K., and Viisanen, Y.: Aerosol measurements at the Gual Pahari EUCAARI station: preliminary results from in-situ measurements, *Atmos. Chem. Phys.*, 10, 7241–7252, doi:10.5194/acp-10-7241-2010, 2010.
- Komppula, M., Lihavainen, H., Hyvärinen, A.-P., Kerminen, V.-M., Panwar, T. S., Sharma, V. P., and Viisanen, Y.: Physical properties of aerosol particles at a Himalayan background site in India, *J. Geophys. Res.*, 114, D12 202, doi:10.1029/2008JD011007, 2009.
- Kondo, Y., Matsui, H., Moteki, N., Sahu, L., Takegawa, N., Kajino, M., Zhao, Y., Cubison, M. J., Jimenez, J. L., Vay, S., Diskin, G. S., Anderson, B., Wisthaler, A., Mikoviny, T., Fuelberg, H. E., Blake, D. R., Huey, G., Weinheimer, A. J., Knapp, D. J., and Brune, W. H.: Emissions of black carbon, organic, and inorganic aerosols from biomass burning in North America and Asia in 2008, *J. Geophys. Res.-Atmos.*, 116, D08 204, doi:10.1029/2010JD015152, 2011.
- Laborde, M., Mertes, P., Zieger, P., Dommen, J., Baltensperger, U., and Gysel, M.: Sensitivity of the Single Particle Soot Photometer to different black carbon types, *Atmos. Meas. Tech.*, 5, 1031–1043, doi:10.5194/amt-5-1031-2012, 2012.
- Lack, D., Moosmüller, H., McMeeking, G., Chakrabarty, R., and Baumgardner, D.: Characterizing elemental, equivalent black, and refractory black carbon aerosol particles: a review of techniques, their limitations and uncertainties, *Anal. Bioanal. Chem.*, 406, 99–122, doi:10.1007/s00216-013-7402-3, 2014.
- Lau, W. K. M., Kim, M.-K., Kim, K.-M., and Lee, W.-S.: Enhanced surface warming and accelerated snow melt in the Himalayas and Tibetan Plateau induced by absorbing aerosols, *Environ. Res. Lett.*, 5, 025 204, 2010.
- Liu, D., Allan, J., Whitehead, J., Young, D., Flynn, M., Coe, H., McFiggans, G., Fleming, Z. L., and Bandy, B.: Ambient black carbon particle hygroscopic properties controlled by mixing state and composition, *Atmos. Chem. Phys.*, 13, 2015–2029, doi:10.5194/acp-13-2015-2013, 2013.

- McMeeking, G. R., Good, N., Petters, M. D., McFiggans, G., and Coe, H.: Influences on the fraction of hydrophobic and hydrophilic black carbon in the atmosphere, *Atmos. Chem. Phys.*, **11**, 5099–5112, doi:10.5194/acp-11-5099-2011, 2011.
- Menon, S., Hansen, J., Nazarenko, L., and Luo, Y.: Climate Effects of Black Carbon Aerosols in China and India, *Science*, **297**, 2250–2253, doi:10.1126/science.1075159, 2002.
- 5 Metcalf, A. R., Craven, J. S., Ensberg, J. J., Brioude, J., Angevine, W., Sorooshian, A., Duong, H. T., Jonsson, H. H., Flagan, R. C., and Seinfeld, J. H.: Black carbon aerosol over the Los Angeles Basin during CalNex, *J. Geophys. Res.-Atmos.*, **117**, D00V13, doi:10.1029/2011JD017255, 2012.
- ~~Moffet, R. C. and Prather, K. A.: In-situ measurements of the mixing state and optical properties of soot with implications for radiative forcing estimates, *P. Natl. Acad. Sci. USA*, **106**, 11 872–11 877, , 2009.~~
- 10 Moteki, N. and Kondo, Y.: Effects of Mixing State on Black Carbon Measurements by Laser-Induced Incandescence, *Aerosol Sci. Tech.*, **41**, 398–417, doi:10.1080/02786820701199728, 2007.
- Moteki, N., Kondo, Y., and Nakamura, S.: Method to measure refractive indices of small nonspherical particles: Application to black carbon particles, *J. Aerosol Sci.*, **41**, 513–521, doi:10.1016/j.jaerosci.2010.02.013, 2010.
- Moteki, N., Kondo, Y., and Adachi, K.: Identification by single-particle soot photometer of black carbon particles attached to other particles: Laboratory experiments and ground observations in Tokyo, *J. Geophys. Res.-Atmos.*, **119**, 1031–1043, doi:10.1002/2013JD020655, 2014.
- 15 Ohata, S., Schwarz, J. P., Moteki, N., Koike, M., Takami, A., and Kondo, Y.: Hygroscopicity of materials internally mixed with black carbon measured in Tokyo, *J. Geophys. Res.-Atmos.*, **121**, 362–381, doi:10.1002/2015JD024153, 2016.
- Pagels, J., Khalizov, A. F., McMurry, P. H., and Zhang, R. Y.: Processing of Soot by Controlled Sulphuric Acid and Water Condensation–Mass and Mobility Relationship, *Aerosol Sci. Tech.*, **43**, 629–640, doi:10.1080/02786820902810685, 2009.
- 20 ~~Park, K., Cao, F., Kittelson, D. B., and McMurry, P. H.: Relationship between Particle Mass and Mobility for Diesel Exhaust Particles, *Environ. Sci. Technol.*, **37**, 577–583, , 2003.~~
- Panwar, T., Hooda, R. K., Lihavainen, H., Hyvärinen, A., Sharma, V., and Viisanen, Y.: Atmospheric aerosols at a regional background Himalayan site–Mukteshwar, India, *Environmental Monitoring and Assessment*, **185**, 4753–4764, doi:10.1007/s10661-012-2902-8, 2013.
- Peng, J., Hu, M., Guo, S., Du, Z., Zheng, J., Shang, D., Levy Zamora, M., Zeng, L., Shao, M., Wu, Y.-S., Zheng, J., Wang, Y., Glen, C. R., Collins, D. R., Molina, M. J., and Zhang, R.: Markedly enhanced absorption and direct radiative forcing of black carbon under polluted urban environments, *P. Natl. Acad. Sci. USA*, **113**, 4266–4271, doi:10.1073/pnas.1602310113, 2016.
- 25 Petzold, A., Ogren, J. A., Fiebig, M., Laj, P., Li, S.-M., Baltensperger, U., Holzer-Popp, T., Kinne, S., Pappalardo, G., Sugimoto, N., Wehrli, C., Wiedensohler, A., and Zhang, X.-Y.: Recommendations for reporting "black carbon" measurements, *Atmos. Chem. Phys.*, **13**, 8365–8379, doi:10.5194/acp-13-8365-2013, 2013.
- 30 Raatikainen, T., Hyvärinen, A.-P., Hatakka, J., Panwar, T., Hooda, R., Sharma, V., and Lihavainen, H.: The effect of boundary layer dynamics on aerosol properties at the Indo-Gangetic plains and at the foothills of the Himalayas, *Atmos. Environ.*, **89**, 548–555, doi:10.1016/j.atmosenv.2014.02.058, 2014.
- Raatikainen, T., Brus, D., Hyvärinen, A.-P., Svensson, J., Asmi, E., and Lihavainen, H.: Black carbon concentrations and mixing state in the Finnish Arctic, *Atmos. Chem. Phys.*, **15**, 10 057–10 070, doi:10.5194/acp-15-10057-2015, 2015.
- 35 Ramanathan, V., Crutzen, P. J., Lelieveld, J., Mitra, A. P., Althausen, D., Anderson, J., Andreae, M. O., Cantrell, W., Cass, G. R., Chung, C. E., Clarke, A. D., Coakley, J. A., Collins, W. D., Conant, W. C., Dulac, F., Heintzenberg, J., Heymsfield, A. J., Holben, B., Howell, S., Hudson, J., Jayaraman, A., Kiehl, J. T., Krishnamurti, T. N., Lubin, D., McFarquhar, G., Novakov, T., and I. A. Podgorny, J. A. O., Prather, K., Priestley, K., Prospero, J. M., Quinn, P. K., Rajeev, K., Rasch, P., Rupert, S., Sadourny, R., Satheesh, S. K., Shaw, G. E., Sheridan,

- P., and Valero, F. P. J.: Indian Ocean Experiment: An integrated analysis of the climate forcing and effects of the great Indo-Asian haze, *J. Geophys. Res.*, 106, 28 371–28 398, 2001.
- Ramanathan, V., Li, F., Ramana, M. V., Praveen, P. S., Kim, D., Corrigan, C. E., Nguyen, H., Stone, E. A., Schauer, J. J., Carmichael, G. R., Adhikary, B., and Yoon, S. C.: Atmospheric brown clouds: Hemispherical and regional variations in long-range transport, absorption, and radiative forcing, *J. Geophys. Res.*, 112, D22S21, doi:10.1029/2006JD008124, 2007.
- 5 Reddington, C. L., McMeeking, G., Mann, G. W., Coe, H., Frontoso, M. G., Liu, D., Flynn, M., Spracklen, D. V., and Carslaw, K. S.: The mass and number size distributions of black carbon aerosol over Europe, *Atmos. Chem. Phys.*, 13, 4917–4939, doi:10.5194/acp-13-4917-2013, 2013.
- Sahu, L. K., Kondo, Y., Moteki, N., Takegawa, N., Zhao, Y., Cubison, M. J., Jimenez, J. L., Vay, S., Diskin, G. S., Wisthaler, A., Mikoviny, T., Huey, L. G., Weinheimer, A. J., and Knapp, D. J.: Emission characteristics of black carbon in anthropogenic and biomass burning plumes over California during ARCTAS-CARB 2008, *J. Geophys. Res.-Atmos.*, 117, doi:10.1029/2011JD017401, 2012.
- 10 Schwarz, J. P., Gao, R. S., Fahey, D. W., Thomson, D. S., Watts, L. A., Wilson, J. C., Reeves, J. M., Darbeheshti, M., Baumgardner, D. G., Kok, G. L., Chung, S. H., Schulz, M., Hendricks, J., Lauer, A., Kärcher, B., Slowik, J. G., Rosenlof, K. H., Thompson, T. L., Langford, A. O., Loewenstein, M., and Aikin, K. C.: Single-particle measurements of midlatitude black carbon and light-scattering aerosols from the boundary layer to the lower stratosphere, *J. Geophys. Res.-Atmos.*, 111, D16 207, doi:10.1029/2006JD007076, 2006.
- 15 Schwarz, J. P., Gao, R. S., Spackman, J. R., Watts, L. A., Thomson, D. S., Fahey, D. W., Ryerson, T. B., Peischl, J., Holloway, J. S., Trainer, M., Frost, G. J., Baynard, T., Lack, D. A., de Gouw, J. A., Warneke, C., and Del Negro, L. A.: Measurement of the mixing state, mass, and optical size of individual black carbon particles in urban and biomass burning emissions, *Geophys. Res. Lett.*, 35, L13 810, doi:10.1029/2008GL033968, 2008.
- 20 Sedlacek, A. J., Lewis, E. R., Kleinman, L., Xu, J., and Zhang, Q.: Determination of and evidence for non-core-shell structure of particles containing black carbon using the Single-Particle Soot Photometer (SP2), *Geophys. Res. Lett.*, 39, L06 802, doi:10.1029/2012GL050905, 2012.
- Slowik, J. G., Cross, E. S., Han, J.-H., Davidovits, P., Onasch, T. B., Jayne, J. T., Williams, L. R., Canagaratna, M. R., Worsnop, D. R., Chakrabarty, R. K., Moosmüller, H., Arnott, W. P., Schwarz, J. P., Gao, R.-S., Fahey, D. W., Kok, G. L., and Petzold, A.: An Inter-Comparison of Instruments Measuring Black Carbon Content of Soot Particles, *Aerosol Sci. Tech.*, 41, 295–314, doi:10.1080/02786820701197078, 2007.
- 25 Sorensen, C. M.: Light Scattering by Fractal Aggregates: A Review, *Aerosol Sci. Tech.*, 35, 648–687, doi:10.1080/02786820117868, 2001.
- Stephens, M., Turner, N., and Sandberg, J.: Particle identification by laser-induced incandescence in a solid-state laser cavity, *Appl. Opt.*, 42, 3726–3736, doi:10.1364/AO.42.003726, 2003.
- 30 Stocker, T., Qin, D., Plattner, G.-K., Tignor, M., Allen, S., Boschung, J., Nauels, A., Xia, Y., Bex, V., and Midgley, P., eds.: *Climate Change 2013: The Physical Science Basis. Contribution of Working Group I to the Fifth Assessment Report of the Intergovernmental Panel on Climate Change*, Cambridge University Press, Cambridge, United Kingdom and New York, NY, USA, 1535 pp., 2013.
- Taylor, J. W., Allan, J. D., Liu, D., Flynn, M., Weber, R., Zhang, X., Lefter, B. L., Grossberg, N., Flynn, J., and Coe, H.: Assessment of the sensitivity of core/shell parameters derived using the single-particle soot photometer to density and refractive index, *Atmos. Meas. Tech.*, 8, 1701–1718, doi:10.5194/amt-8-1701-2015, 2015.
- 35 ~~Weber, A. P., Baltensperger, U., Gögeler, H. W. and Schmidt-Ott, A.: In-situ characterization and structure modification of agglomerated aerosol particles, *J. Aerosol Sci.*, 27, 915–929, doi:10.1016/0021-8502(96)00013-4, 1996.~~

- Wang, Q., Schwarz, J. P., Cao, J., Gao, R., Fahey, D. W., Hu, T., Huang, R.-J., Han, Y. and Shen, Z.: Black carbon aerosol characterization in a remote area of Qinghai–Tibetan Plateau, western China, *Sci. Total Environ.*, 1, 151–158, doi:10.1016/j.scitotenv.2014.01.098, 2014.
- Wiedensohler, A., Birmili, W., Nowak, A., Sonntag, A., Weinhold, K., Merkel, M., Wehner, B., Tuch, T., Pfeifer, S., Fiebig, M., Fjåraa, A. M., Asmi, E., Sellegri, K., Depuy, R., Venzac, H., Villani, P., Laj, P., Aalto, P., Ogren, J. A., Swietlicki, E., Williams, P., Roldin, P., 5 Quincey, P., Hüglin, C., Fierz-Schmidhauser, R., Gysel, M., Weingartner, E., Riccobono, F., Santos, S., Grüning, C., Faloon, K., Beddows, D., Harrison, R., Monahan, C., Jennings, S. G., O’Dowd, C. D., Marinoni, A., Horn, H.-G., Keck, L., Jiang, J., Scheckman, J., McMurry, P. H., Deng, Z., Zhao, C. S., Moerman, M., Henzing, B., de Leeuw, G., Löschau, G., and Bastian, S.: Mobility particle size spectrometers: harmonization of technical standards and data structure to facilitate high quality long-term observations of atmospheric particle number size distributions, *Atmos. Meas. Tech.*, 5, 657–685, doi:10.5194/amt-5-657-2012, 2012.
- 10 Zhang, R., Khalizov, A. F., Pagels, J., Zhang, D., Xue, H., and McMurry, P. H.: Variability in morphology, hygroscopicity, and optical properties of soot aerosols during atmospheric processing, *P. Natl. Acad. Sci. USA*, 105, 10 291–10 296, doi:10.1073/pnas.0804860105, 2008.
- Zhang, Y., Zhang, Q., Cheng, Y., Su, H., Kecorius, S., Wang, Z., Wu, Z., Hu, M., Zhu, T., Wiedensohler, A., and He, K.: Measuring the morphology and density of internally mixed black carbon with SP2 and VTDMA: new insight into the absorption enhancement of black 15 carbon in the atmosphere, *Atmos. Meas. Tech.*, 9, 1833–1843, doi:10.5194/amt-9-1833-2016, 2016.

Table 1. Campaign average values (\pm standard deviations) describing rBC mass size distributions (total mass and geometric mass mean diameter and standard deviation) and mixing state (number and volume mean core diameters, those normalized by the mobility size (D_m), and number fraction of particles containing rBC). The mixing state parameters are calculated for the 360 nm mobility size bins.

Parameter	Gual Pahari	Mukteshwar
Total rBC ($\mu\text{g m}^{-3}$)	11 ± 11	1.0 ± 0.6
GMD $\text{dm}/\text{dlog}D_{\text{rBC}}$ (nm)	249 ± 30	217 ± 13
GSD $\text{dm}/\text{dlog}D_{\text{rBC}}$	0.246 ± 0.014	0.221 ± 0.014
$D_{\text{rBC},\text{N}}$ (nm)	185 ± 8	178 ± 12
$D_{\text{rBC},\text{N}}/D_m$	0.51 ± 0.02	0.50 ± 0.03
$D_{\text{rBC},\text{V}}$ (nm)	221 ± 14	205 ± 16
$D_{\text{rBC},\text{V}}/D_m$	0.61 ± 0.04	0.57 ± 0.04
$N_{\text{rBC}}/N_{\text{total}}$	0.46 ± 0.12	0.31 ± 0.05



Figure 1. Locations of Gual Pahari (red marker) and Mukteshwar (blue marker) measurement stations.

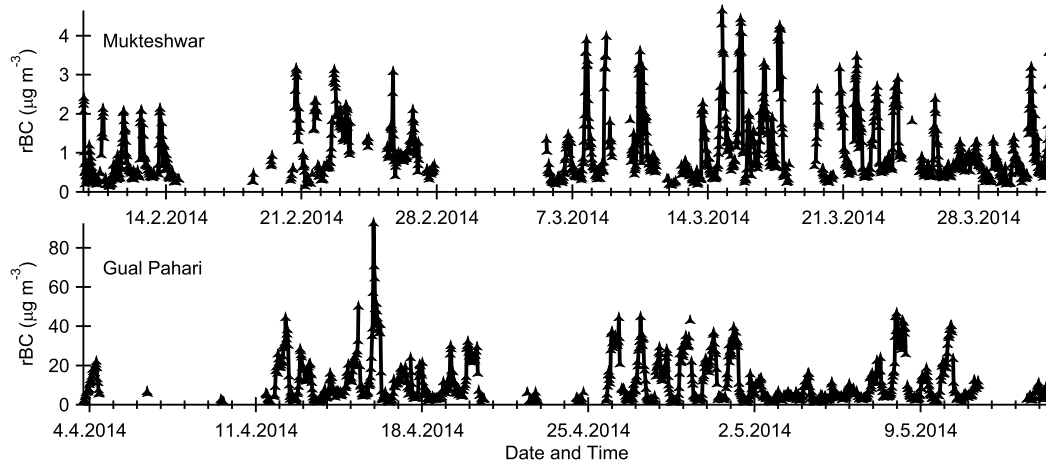


Figure 2. Total rBC mass concentration time series from Mukteshwar (top graph) and Gual Pahari (bottom graph).

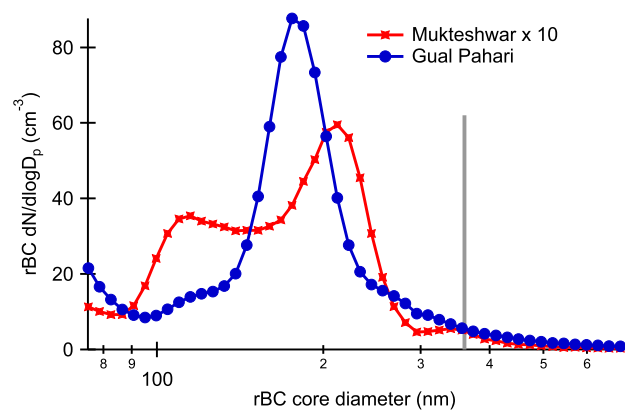


Figure 3. Campaign average rBC core number size distributions for the 360 nm DMA-selected mobility diameter (indicated by the vertical gray line) from Mukteshwar (multiplied by a factor of ten) and Gual Pahari. Standard deviations are approximately equal with the average concentration values when concentrations are larger than 1 cm^{-3} while smaller concentrations mean increasing standard deviations.

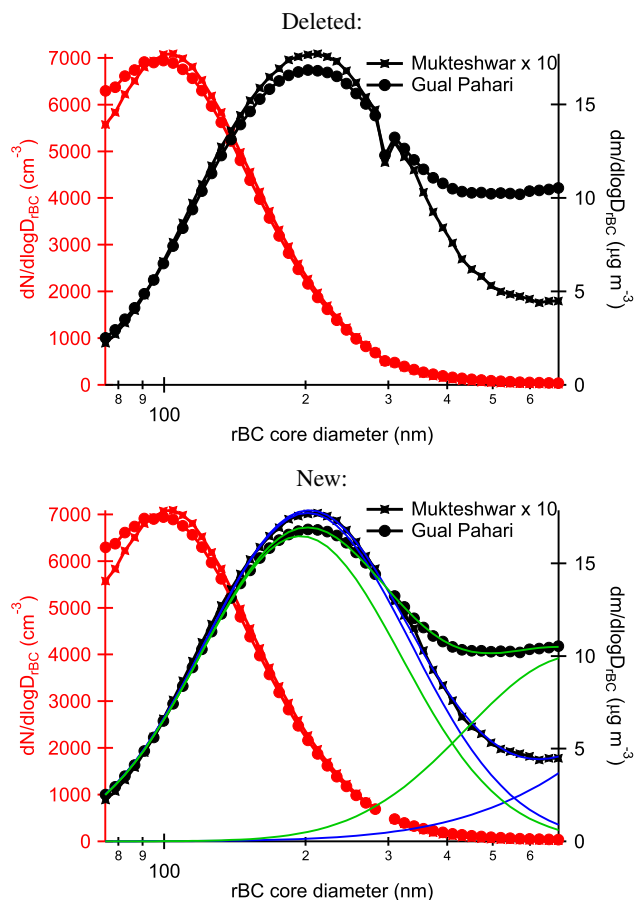


Figure 4. Campaign average rBC mass (black color, right axis) and number (red color, left axis) size distributions for Mukteshwar (lines with circles) and Gual Pahari (lines with crosses). The thin lines are bimodal log-normal fits including both modes and the total fitted mass (blue line for Mukteshwar and green line for Gual Pahari). Mukteshwar number and mass size distributions have been multiplied by a factor of ten. Standard deviations are approximately 80 % (Mukteshwar) or 100 % (Gual Pahari) of the bin mean number and mass. The gap at about 300 nm is caused by discontinuous high and low gain rBC mass calibration parameterizations.

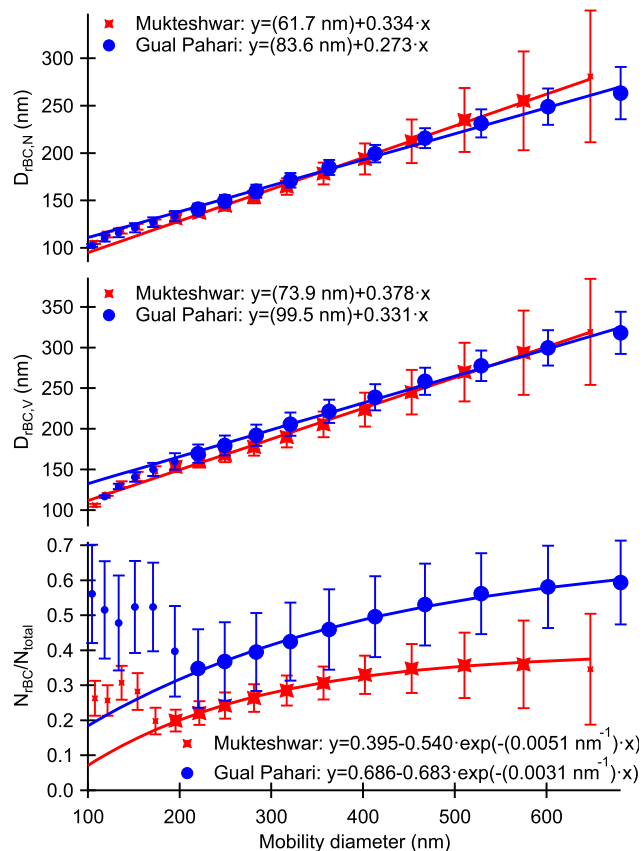


Figure 5. Size dependent rBC mixing state parameters for Gual Pahari and Mukteshwar. The upper panel shows the number mean rBC core volume equivalent diameters and the mid panel shows those based on the rBC volume. The lower panel shows rBC particle number fractions. Solid lines are the fits to the data (ignoring bad data points with indicated by the smaller marker size). Error bars indicate ± 1 standard deviation limits.

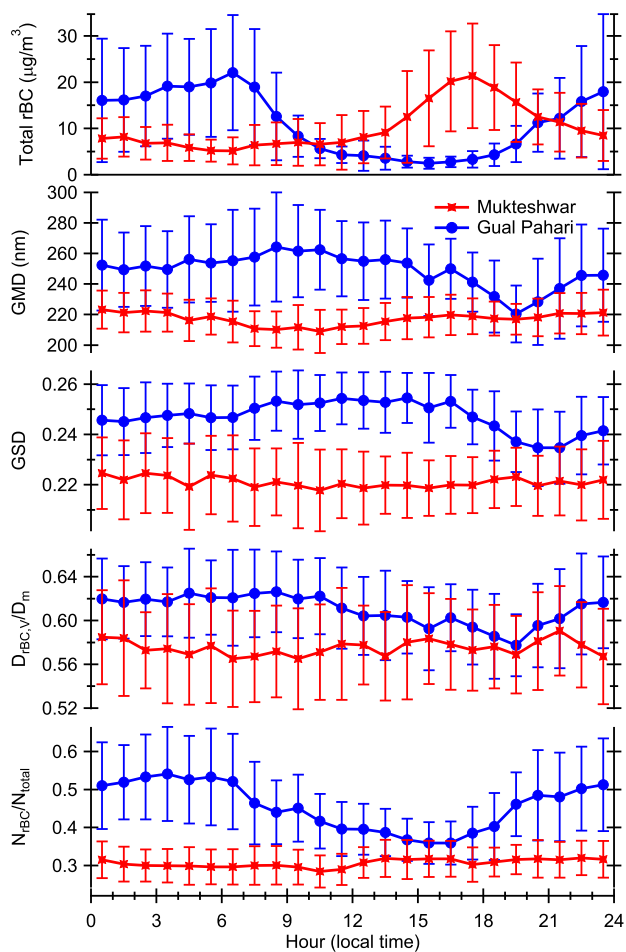


Figure 6. Diurnal cycles of rBC core mass size distribution parameters (total mass concentrations and geometric mass mean diameter and standard deviation), rBC core to mobility diameter ratios and fractions of particles containing rBC. The diameter ratios and fractions are calculated for the 360 nm mobility size. Error bars indicate ± 1 standard deviation limits. Mukteshwar total rBC mass concentration and its standard deviation have been multiplied by a factor of ten.

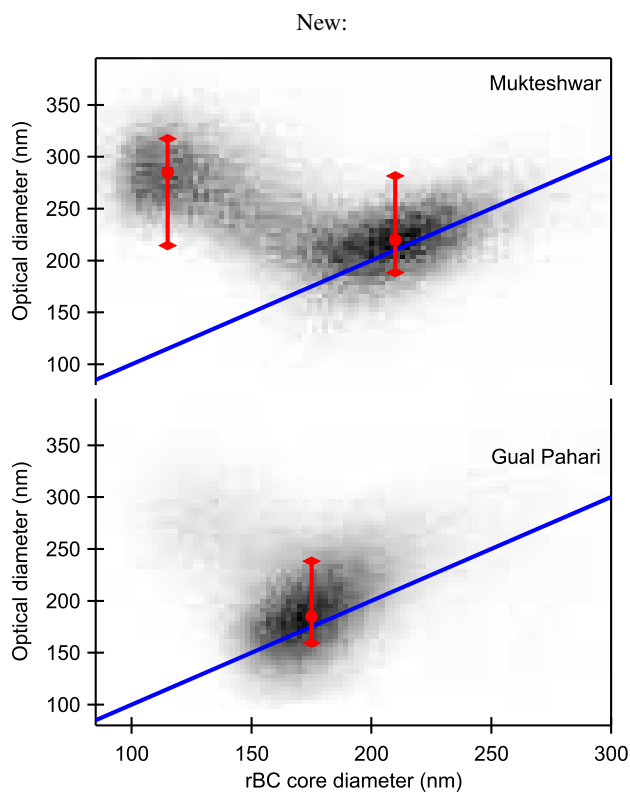
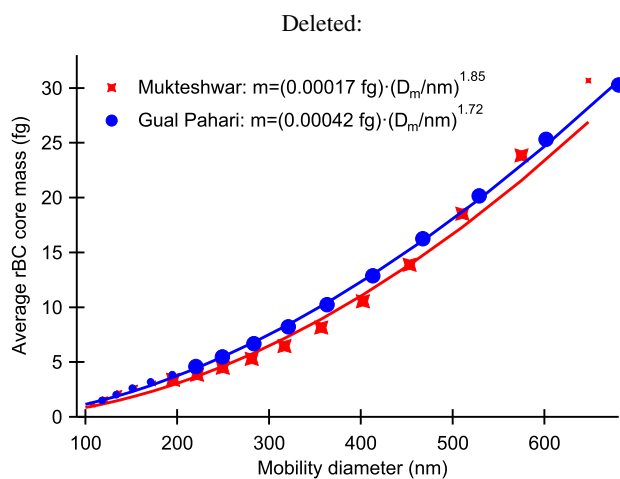


Figure 7. Campaign average rBC core mass as a function of mobility diameter and fits to the observations (ignoring points with smaller marker size) Distributions of single particle optical and rBC core diameters for the 360 nm mobility size and 30–35 °C instrument temperature range (darker color indicates higher probability). The blue lines indicate equal rBC and optical diameters. The red markers represent the mode center points and the error bars are based on calculations using different optical constants (ammonium sulfate and rBC).

Supplementary material:

1 Instrument setup

The both Gual Pahari and Mukteshwar measurements we conducted using a Differential Mobility Particle Sizer (DMPS) coupled with a SP2 (Fig. S1). The DMPS is composed of a Differential Mobility Analyzer (DMA; medium HAUKE-type, with a bipolar radioactive (Am) neutralizer) and a Condensation Particle Counter (CPC; TSI model 3010, TSI Inc. USA). A polydisperse ambient aerosol population is dried (first drier (using silica-gel, Sigma Aldrich) was in main inlet line outside, second stage was 1 meter-long nafion drier (Perma Pure) inside the building, third drier (silica-gel, Sigma Aldrich) was in closed DMA sheath flow loop) and the charge distribution is neutralized before entering the DMA where a narrow particle size range is selected based on a voltage control (VDC) while keeping the constant flow rates (both sheath and aerosol sample: Q_a). The size-selected aerosol is then lead to the CPC, which measured the total number concentration of particles (N_{total}). The SP2 was connected in parallel to the CPC where the SP2 measures the number concentrations of all particles (N_{total}) and also those containing refractory material (N_{rBC}), which is assumed to be refractory black carbon (rBC). In addition, the SP2 measures particle sizes and the mass of refractory material (m_{rBC}) in each particle. Particle size measured by the SP2 is only used mainly as a diagnostic parameter; for spherical particles it should be the same as the mobility size selected by the DMA, which is used in the calculations. rBC core volume equivalent diameters (assuming a compact spherical rBC “core” with 1800 kg m^{-3} density) were calculated from the measured rBC mass; it represents the volume fraction of rBC in each absorbing particle.

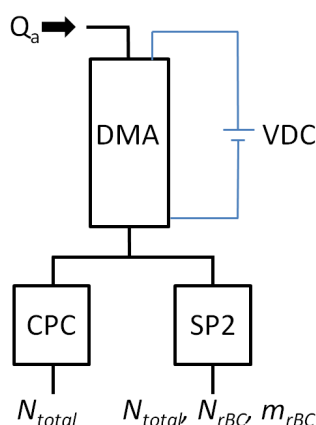


Figure S1: Schematics of the measurement setup.

The DMA voltages are changed stepwise through selected voltage range. Here 30 voltage settings were selected so that logarithmically spaced particle size bins ranged from about 20 to 650 nm (there were small fluctuations due to instrument temperature and pressure changes). The time step was initially set to 30 s, but it was later increased to 60 s to improve the SP2 counting statistics. As a result, the full scan with 60 s time step took 32 minutes.

The CPC and SP2 data were aligned visually. The CPC data is automatically saved as an average concentration for each time step, but this was done manually for the SP2 data where the relevant parameters are number concentrations for all particles and those containing rBC (used to calculate the number fraction of particles containing rBC), and rBC core size distributions which are here represented by suitable distribution parameters. These were calculated using the standard instrument calibration and data analysis methods (see below). The first measurements showed that the rBC core size distributions are not always narrow and unimodal, which means that the commonly used number mean rBC core diameter is

smaller than the corresponding mass mean diameter. For consistency with the further mass calculations, both mass and number mean diameters were saved.

1.1 SP2 calibration

The maximum incandescence and scattering signals are proportional to the refractory particle mass and the total particle size, respectively, and these dependencies are parameterized using suitable calibration reference materials. Our regular incandescence calibrations are based on size-selected Aquadag (Acheson Inc., USA) particles which masses are calculated using the density parameterization from Gysel et al. (2011). Several studies have shown that fullerene soot is the best representative of ambient rBC and its incandescence signal is about 75% of that of Aquadag with the same particle mass (Moteki and Kondo, 2010; Kondo et al., 2011; Gysel et al., 2011; Baumgardner et al., 2012; Laborde et al., 2012). Therefore, Aquadag incandescence amplitudes were multiplied by a factor of 0.75 to make it representative of the fullerene soot and ambient rBC. This fullerene soot-equivalent calibration gives ambient rBC particle mass as a function of the measured maximum incandescence signal. rBC core volume equivalent diameters (briefly: rBC core diameter) are then calculated by assuming a compact spherical “core” with 1800 kg m^{-3} density. The sizing limits for the refractory material are 0.3-380 fg for rBC mass and 70-740 nm for the rBC core diameter.

~~Because particle sizes are accurately selected by the DMA especially for rBC-containing particles, scattering sizes measured by the SP2 are mainly used for diagnostic purposes. Although we do not use scattering sizes measured by the SP2 (these are accurately selected by the DMA especially for absorbing particles), we calculate those for diagnostic purposes.~~ Our regular scattering size calibrations are based on size-selected ammonium sulfate, but here we can also use size-selected ambient particles. The instrument was calibrated using ammonium sulfate before shipping to India (December 13, 2013), but not during the campaign. Scattering amplitudes from the ammonium sulfate calibration and Mukteshwar observations (February 9, 2014) are almost identical with only 3% difference in particle size. Such a small difference can be easily caused by the difference in optical properties of ammonium sulfate and ambient particles or minor changes in the instrument performance. However, significant reduction in scattering signal (equivalent to 17% increase in particle size) is observed after the instrument was moved to Gual Pahari (data from April 11, 2014). This is most likely caused by decreased laser beam intensity (Laborde et al., 2012). In order to remove this constant sizing bias, Gual Pahari scattering calibration is based on field measurements (data from April 11, 2014). [More details about the laser power is given in later in Sect. 3.4.](#)

2 Data analysis

Just as in a typical DMPS data analysis, ambient size distributions need to be calculated from the raw observations of particle number versus voltage using an inversion code. This inversion depends mainly on particle charging efficiencies and the DMA transfer function. For the DMPS system we have used a standard pseudo-inverse method (see the FMI DMPS inversion description in Wiedensohler et al., 2012), but this method cannot be directly applied to the SP2 data. The main reason is that the SP2 cannot detect small particles (minimum rBC size is about 70 nm and that for scattering particles is roughly 180 nm), which means that ~~multiply charged particles dominate these size bins a large fraction of the size scan particle counts are originating from multiply charged particles.~~ To avoid problems with the data inversion, SP2 size distributions ($dN_{\text{SP2}}/d\log D_p$) concentrations are calculated by multiplying the raw particle number concentrations (N_{SP2}) by the ratio of the inverted DMPS number size distribution ($dN_{\text{DMPS}}/d\log D_p$) to the original using the inversion results particle concentrations from the CPC (N_{CPC}): $dN_{\text{SP2}}/d\log D_p =$

$N_{SP2} \cdot (dN_{DMPS}/d\log D_p)/N_{CPC}$ from DMPS. It would have been possible to convert the time and size dependent particle number concentrations measured by the SP2 (N_{SP2}) to corresponding number size distributions ($dN_{SP2}/d\log D_p$) by multiplying these with the ratio of the DMPS number size distribution ($dN_{DMPS}/d\log D_p$) to the CPC concentration (N_{CPC}). However, in order to reduce noise from the inversion and to make SP2 results less dependent on the CPC data, we have used calculated the modes of the DMPS size distribution to the CPC concentration ratio the correction factor $((dN_{DMPS}/d\log D_p)/N_{CPC})$, which means constant correction for each DMA size. This method is essentially the same as taking a typical DMPS scan and calculating the inversion from that. Figure S2 shows an example of the SP2 inversion method. The red markers are the individual time and size dependent values of $(dN_{DMPS}/d\log D_p)/N_{CPC}$ and blue lines and markers represent the mode, which is the size dependent correction factor ~~inversion~~ for the SP2 concentrations (here number concentrations of particles with and without rBC, rBC mass concentrations, and rBC core number size distributions for the 360 nm mobility size bin).

Parameters calculated for each DMA size like the average rBC core diameter, and scattering particle size and number fraction of rBC-containing-absorbing particles are independent of particle concentrations, so inversion is not needed. Multiply charged particles have a small effect on rBC core diameters (see Fig. S14), but the exact quantification of their contribution or a correction would have required accurate identification of those particles, which is not possible. The average parameters are just averages of those of the individual particles observed during each 30 or 60 s time step. The number fraction is calculated using the corresponding integrated number concentrations.

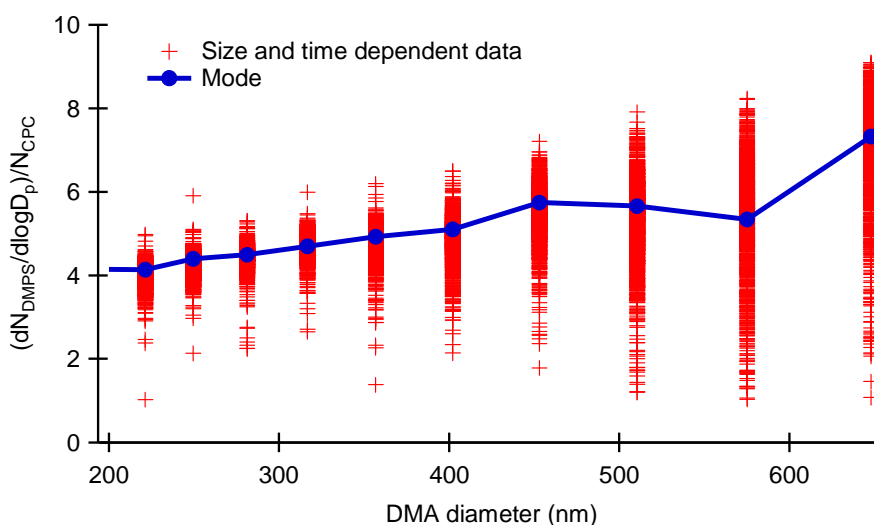


Figure S2: Size and time dependent ratios of the DMPS number size distribution ($dN_{DMPS}/d\log D_p$) to the CPC concentration (N_{CPC}) from Mukteshwar measurements. The blue line and the markers (mode for each DMA diameter) show the size dependent inversion for calculating concentration from SP2 data.

3 Consistency tests

Since this is a new method, tests were made to confirm the validity of the results. First of all, CPC and SP2 total (absorbing + non-absorbing all particles including those that saturate the detectors) number concentrations (used without inversion) should be equal for all DMA sizes larger than about 200 nm, which is larger than the SP2 detection limit for scattering particles. Secondly, the DMA-selected and non-rBC non-absorbing particle mean diameters should be almost identical. Any fluctuation in concentration or size

could mean fluctuations in SP2 performance; the DMA and CPC could have problems too, but these are generally highly stable instruments. After thatFinally, the total rBC mass concentrations are compared with equivalent black carbon (eBC) measured by a 7-wavelength Aethalometer in Mukteshwar. Finally, we diagnose SP2 laser power changes.

3.1 Number concentrations

Figure S3 shows the ratio of CPC and SP2 total ~~(scattering + absorbing)~~ number concentrations as a function of DMA size. The DMA size was limited to 200-420 nm size range, because scattering particle detection limit is close to 200 nm and low particle counts increase noise at sizes larger than 450 nm. Although the number concentrations are correlated, there seems to be a constant bias between CPC readings and total concentrations from the SP2. The CPC readings are consistently about 82 % of those of the SP2 at both sites. There are reasons that could cause such differences, but the typical explanations were ruled out (instruments were working correctly, concentrations were low enough to avoid coincidence counting errors and flow rates were calibrated for both instruments). Further tests with other CPC and SP2 showed the SP2 used in these India measurements is always showing larger number concentrations (the reason for this is currently unknown). ~~Because CPC is a commonly used and robust instrument, it is expected that the SP2 over counts possibly due to a higher flow rate than expected.~~ Therefore, all SP2 mass and number concentration values are here multiplied by a factor of 0.82. With this correction CPC and SP2 results become practically identical.

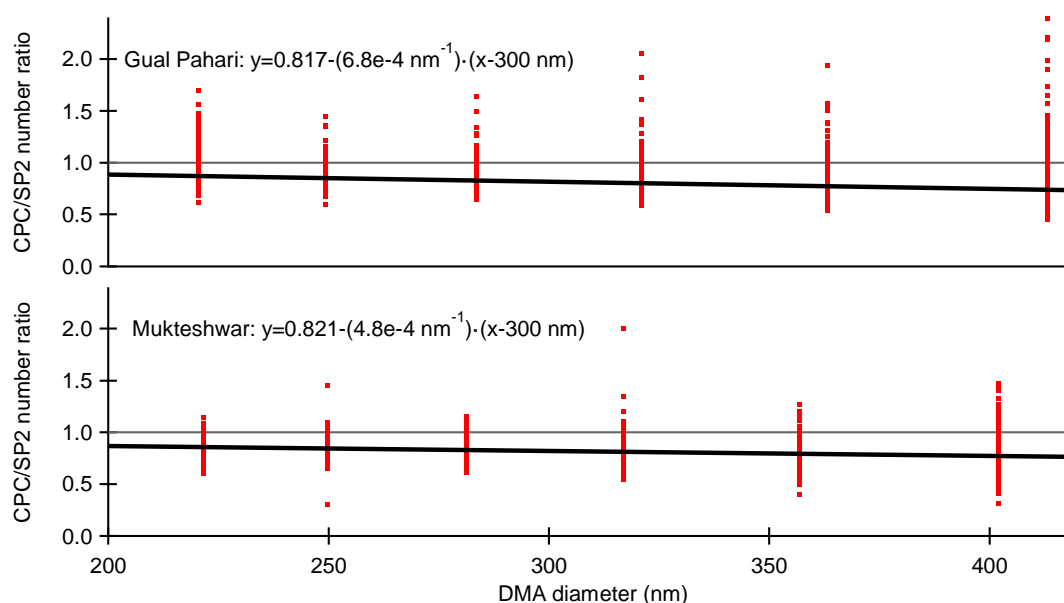


Figure S3: The CPC to total number concentration ratios as a function of DMA size for both Gual Pahari and Mukteshwar. Also shown are the linear fits to the data. The highest number ratios (about 4 for Gual Pahari) are not shown.

The figure above shows that there is some variability in the ratios, but a closer look shows that much of this variability is actually time-dependent. Furthermore, these time-dependent variations correlate with the SP2 chamber temperature. Figure S4 shows the number ratio for about 285 nm DMA diameter as a function of chamber temperature from both measurements campaigns. SP2 chamber temperature depends strongly on the temperature of the air-conditioned measurement building, but less on the ambient temperature. This indicates that the difference in particle number concentration is most likely caused by the SP2.

Although temperature dependent bias correction could be applied to SP2 concentrations, a constant correction is considered to be more robust. The remaining temperature dependent bias introduces some additional noise to the mass and number concentrations, but there is no systematic error since SP2 temperature variations are not following a frequent cycle. Specifically, if the SP2 temperature would have been following the ambient temperature, the observed diurnal cycles would have been affected.

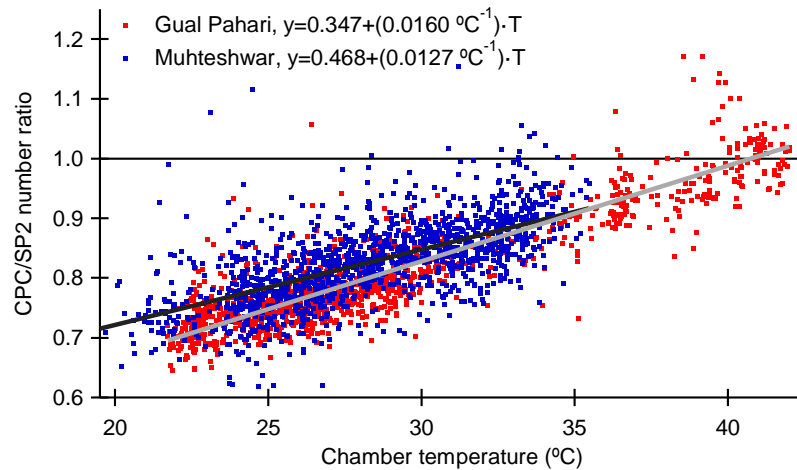


Figure S4: CPC to SP2 total number concentration ratios for 285 nm DMA size for both Gual Pahari and Mukteshwar. Also shown are the linear fits to the data. Clear outliers are not shown.

3.2 Particle sizes

Figure S5 shows the ratio of DMA selected size to those measured by the SP2 as a function of DMA size. The SP2 derived particle sizes are geometric mean diameters of the observed non-[rBCabsorbing](#) particle distributions (determined by fitting a log-normal size distribution to the observed size distributions). Because scattering calibration is based on ambient particles, the average sizing bias is only about 1%.

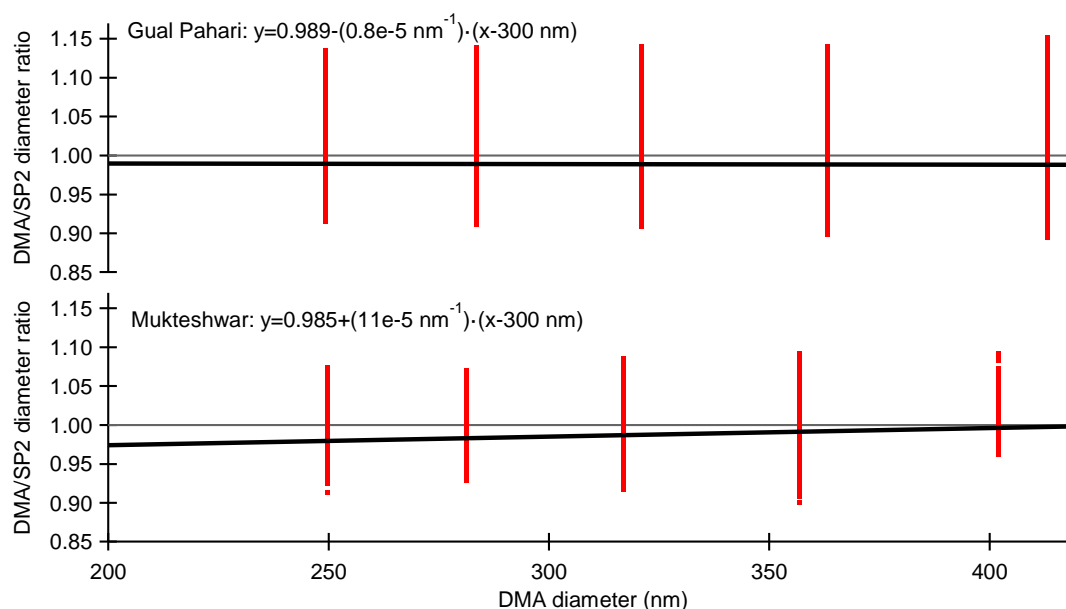


Figure S5: The DMA to scattering diameter ratios as a function of DMA size for both Gual Pahari and Mukteshwar. Also shown are the linear fits to the data.

Although the average sizing bias is negligible (about 1 %) and the bias is independent of particle size (slope in the order of 10^{-5} nm^{-1}), there is some variability in the calculated scattering sizes (about $\pm 10\%$ difference from the DMA-selected size). Again, it seems that the variability in scattering size is related to the variability of the SP2 chamber temperature (Fig. S6), but the dependency is weaker than in the case of concentrations (Fig. S4). In general, this about 10 % sizing uncertainty is within the typically reported sizing uncertainty limits (e.g. Laborde et al., 2012).

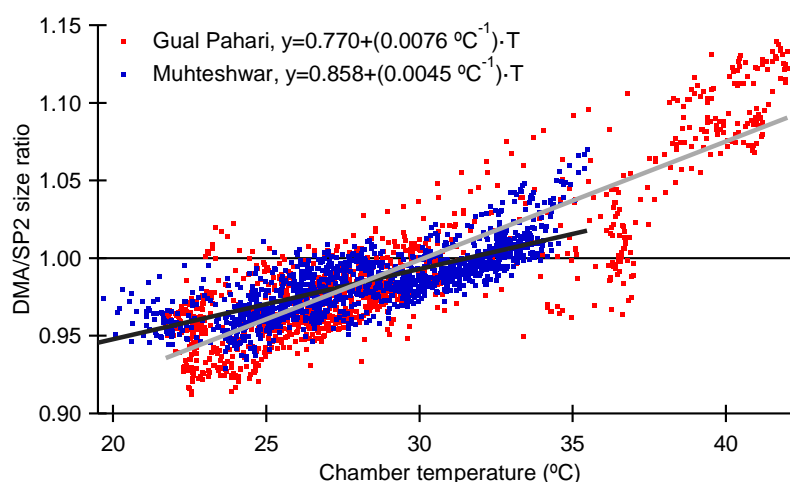


Figure S6: DMA to scattering diameter ratios for 285 nm DMA size for both Gual Pahari and Mukteshwar. Also shown are the linear fits to the data. [Clear outliers are not shown.](#)

3.3 Refractory and equivalent Black Carbon

The Aethalometer collects particles to a filter and measures the change in light attenuation due to the accumulated absorbing aerosol mass (Hansen et al., 1984). The mass concentration of the absorbing aerosol is then calculated from the attenuation and is reported as an equivalent black carbon (eBC). Since this is only a consistency test, the Aethalometer data, which is available for Mukteshwar only (Hyvärinen et al., 2009), is used without typical corrections (e.g. Weingartner et al. 2003), which means that the absolute eBC values are uncertain. Even when the absolute rBC and eBC values are not directly comparable, Figure S7 shows that eBC and rBC are correlated in excellent agreement considering their different measurement methods. Figure S8 also shows that the eBC/rBC ratio is independent of SP2 temperature. This supports the decision that temperature dependent correction is not needed for SP2.

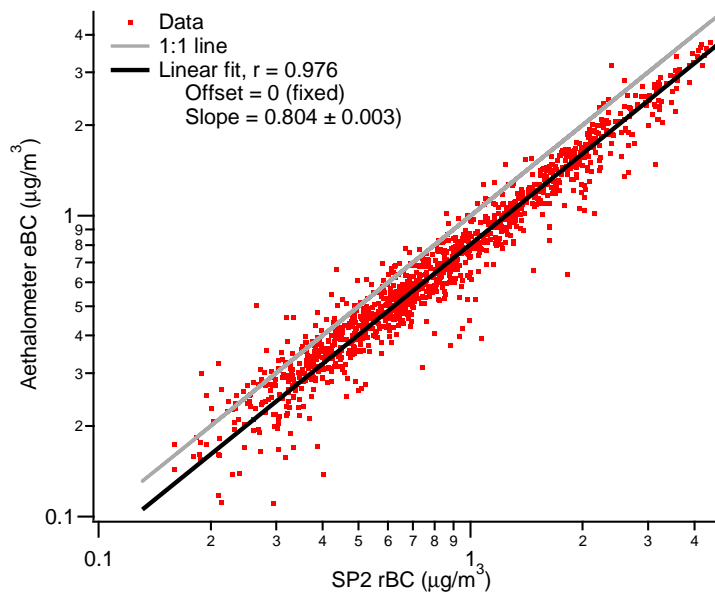


Figure S7: Aethalometer eBC as a function of SP2 rBC and linear fit to data (clear outliers not shown).

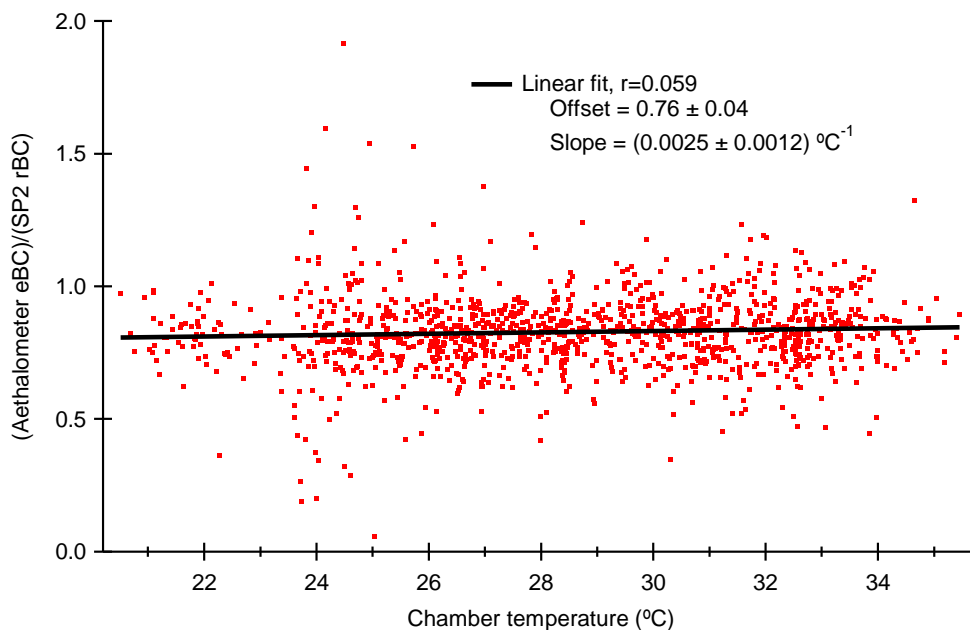


Figure S8: The ratio of Aethalometer eBC to SP2 rBC as a function of SP2 chamber temperature (outliers not shown). Also shown is a linear fit to the data.

3.4 Laser power diagnostics

Figure S9 shows the development of the low gain scattering signal amplitudes for the 285 nm DMA size during the whole measurement period (blue and red marker colors represent Mukteshwar and Gual Pahari, respectively). Also shown is the chamber temperature, which can explain most fluctuations in scattering amplitudes (and particle sizes as shown above). The normalization is based on scattering calibration made just before sending the instrument to India (13.12.2013). On the average, the scattering signals in Mukteshwar and Gual Pahari are reduced to 93% and 41% from the calibration level. The reason for the decrease in the scattering signal when the instrument was transported from Mukteshwar to Gual Pahari is unknown, but it is possible that laser power has decreased.

Too low laser power could mean that rBC in the smallest and/or thickly coated particles is not detected. This is examined by calculating the positions for the maximum incandescence signal. The maximum incandescence signal should be seen before particles cross the laser beam center. Figure S10 shows the distributions of times from incandescence signal to the laser beam center for different mobility diameters and rBC core diameters (half of the mobility diameter ± 5 nm). Variable core sizes were selected so that these would be representative of the typical particles. The data has been selected from one day with low scattering signal amplitudes. Figure S10 shows that laser power is high enough for particles with mobility diameter at least 220 nm (rBC core diameter 110 nm). Smaller mobility diameters and rBC cores may have reduced detection efficiency especially in Gual Pahari. The 200 nm mobility size limit used in the main text is therefore suitable for rBC.

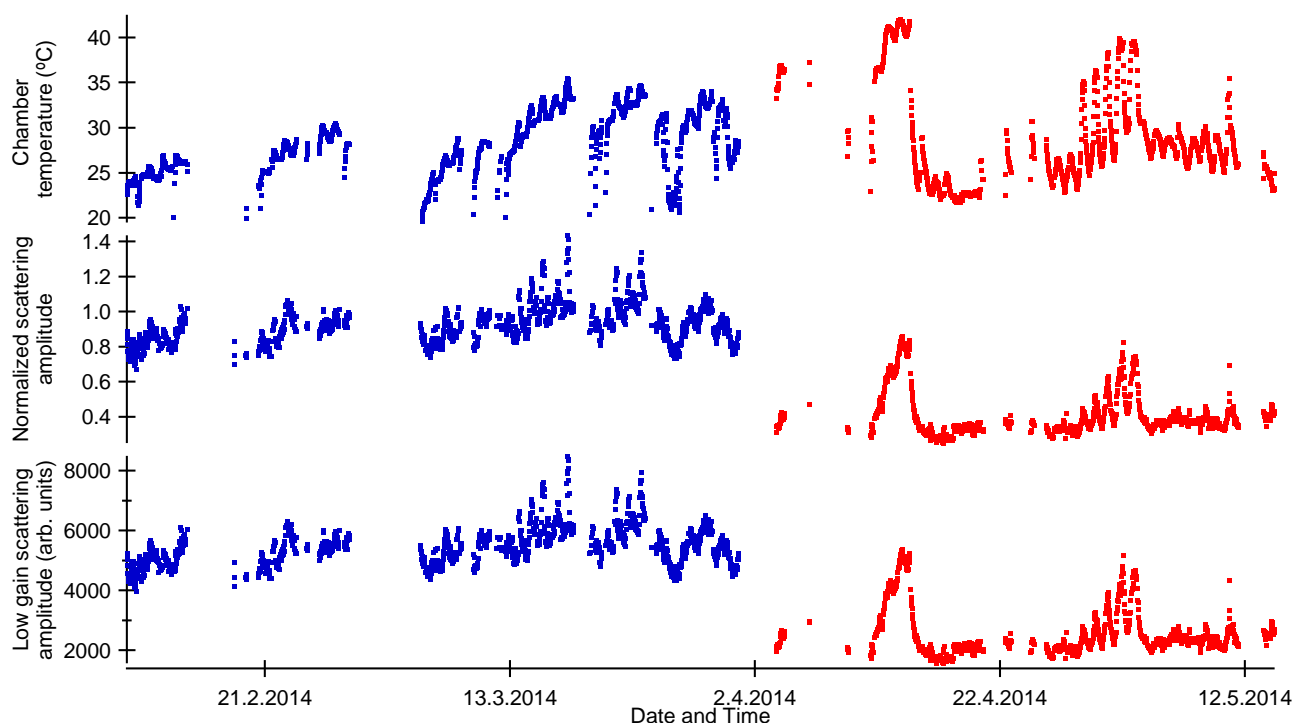


Figure S9: SP2 chamber temperature and measured and normalized scattering amplitudes for Mukteshwar (blue markers) and Gual Pahari (red markers). Scattering amplitudes are for the 285 nm DMA size. The normalization is based on scattering calibration made before sending the instrument to India (13.12.2013).

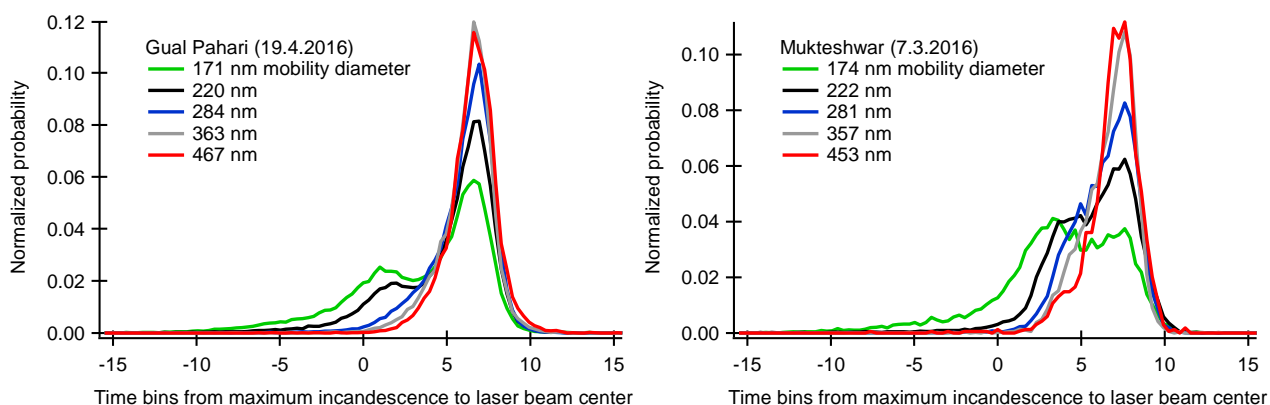
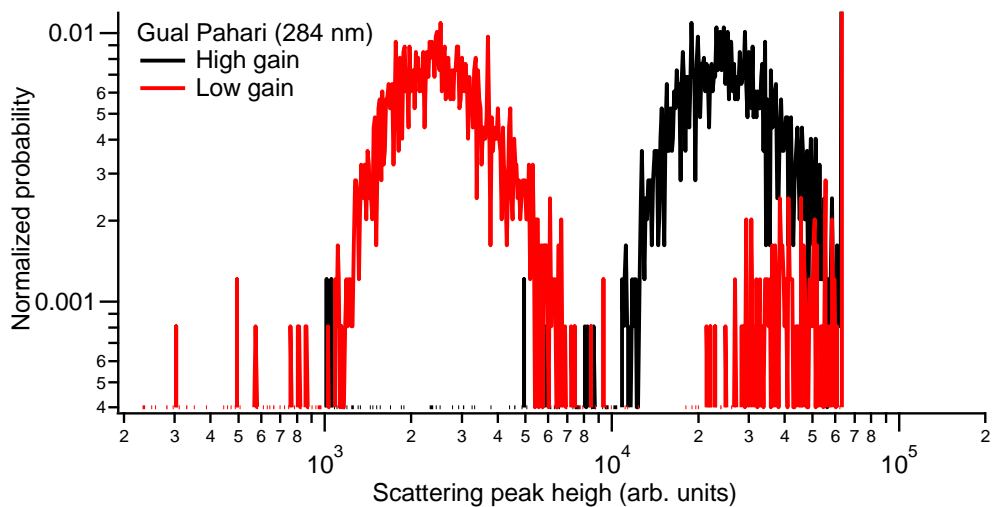


Figure S10: Normalized distributions of incandescence to laser beam center time bins for Gual Pahari and Mukteshwar. The distributions are shown for different mobility and rBC core diameters (core diameter is half of the mobility diameter).

Significant problems with laser could also affect scattering peak height distributions, but such problems were not seen. As an example, scattering peak height distribution for the 285 nm mobility size bin is shown in Fig. S11 for both Gual Pahari (top) and Mukteshwar (bottom). The maximum peak height for the current instrument is about 65000 (depends on the baseline noise) and the peak close to this limit corresponds to saturated signal. As is already shown in Fig. S9, scattering amplitudes are somewhat lower in Gual Pahari.



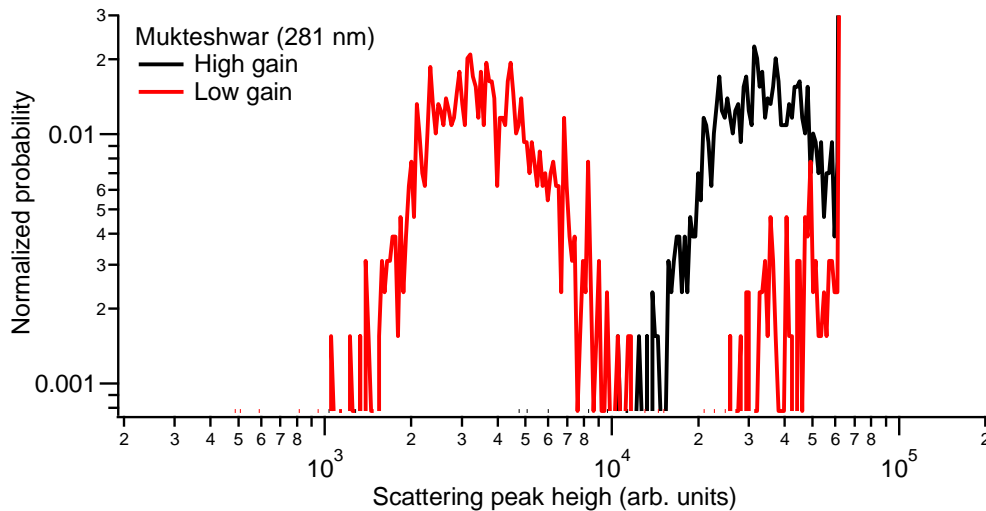


Figure S11: Scattering peak height distributions for 280 nm mobility size for Gual Pahari (top) and Mukteshwar (bottom).

4 Supplementary figures

In addition to the average rBC mass size distributions (total mass and geometric mass mean diameter and standard deviation) and mixing state (number and volume mean core diameters, those normalized by the mobility size, and number fraction of particles containing rBC) parameters for the 360 nm mobility size bins given in the main text (Table 1), figures S102 and S113 show the time series of these parameters (except number and volume mean core diameters as these are proportional to the normalized values).

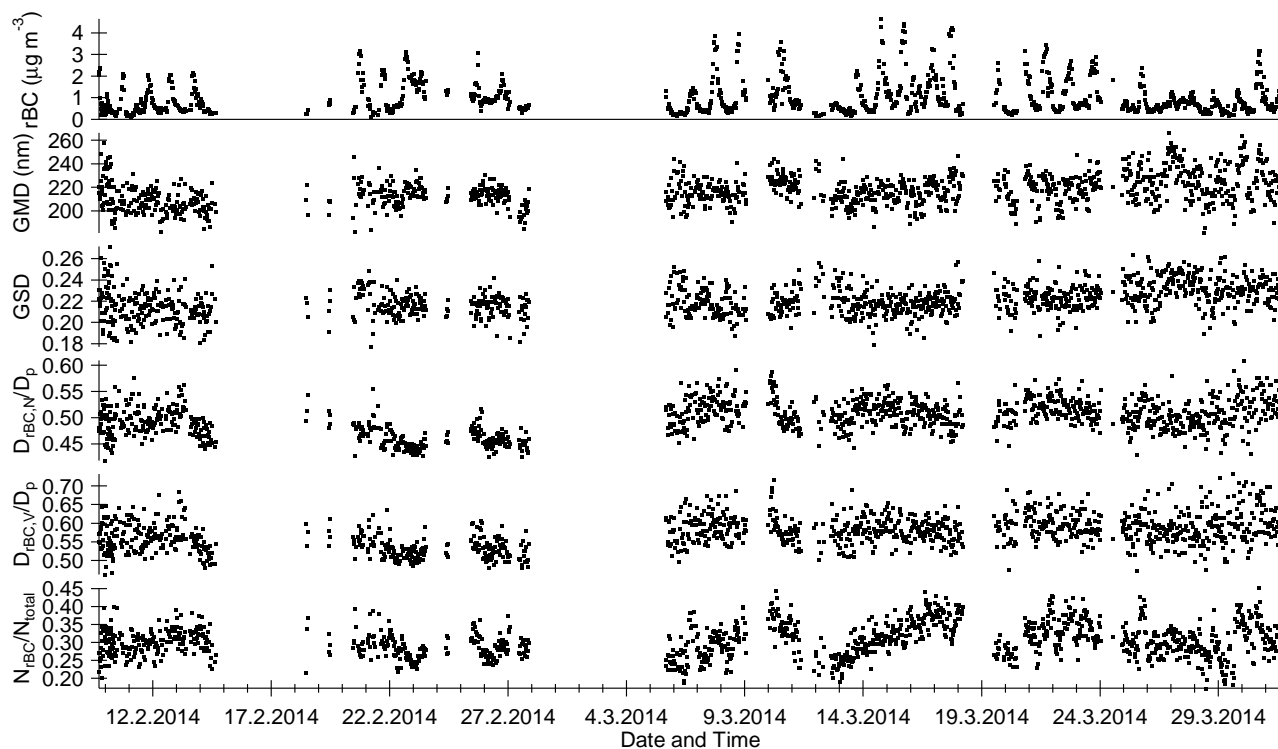


Figure S102: Time series of the measured rBC mass size distribution parameters (total rBC concentration and geometric mass mean diameter and standard deviation) and mixing state parameters (rBC core volume equivalent diameter (both number and volume averages) to mobility particle diameter ratio and number fraction of particles containing rBC) for Mukteshwar.

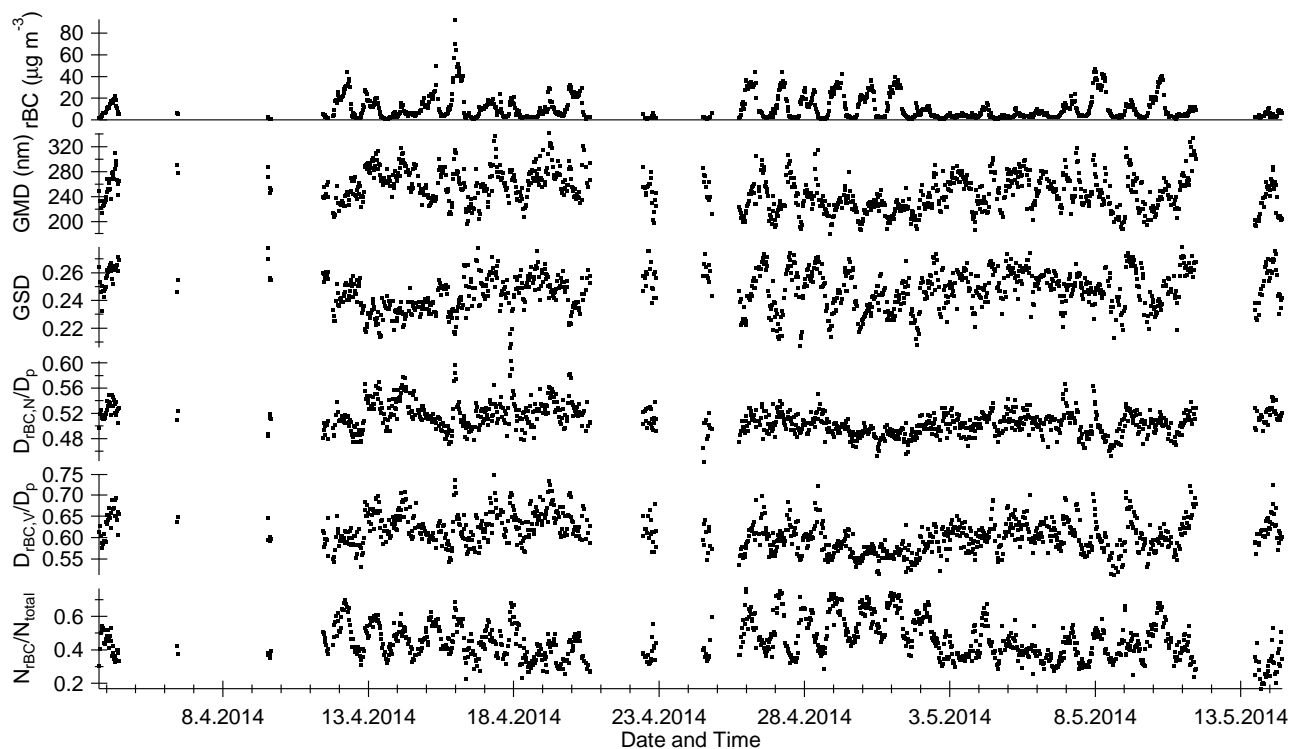


Figure S113: Same as Fig. S102, but for Gual Pahari

Figure 3 in the main text shows the campaign average rBC core number size distributions for the 360 nm DMA-selected mobility diameter. Here Fig. S14 shows the core number size distributions for 220 nm, 360 nm and 520 nm mobility diameters and also with one standard deviation error bars. The 360 nm figure is the same as in the main text, but now with the error bars, and the other two sizes represent the lower and upper limits for accurate measurements. As mentioned in the main text, the mode with smaller rBC cores observed in Mukteshwar is below the detection limit (70 nm) for the measurements with 220 nm mobility diameter. The error bars represent the variability of the rBC mass concentrations.

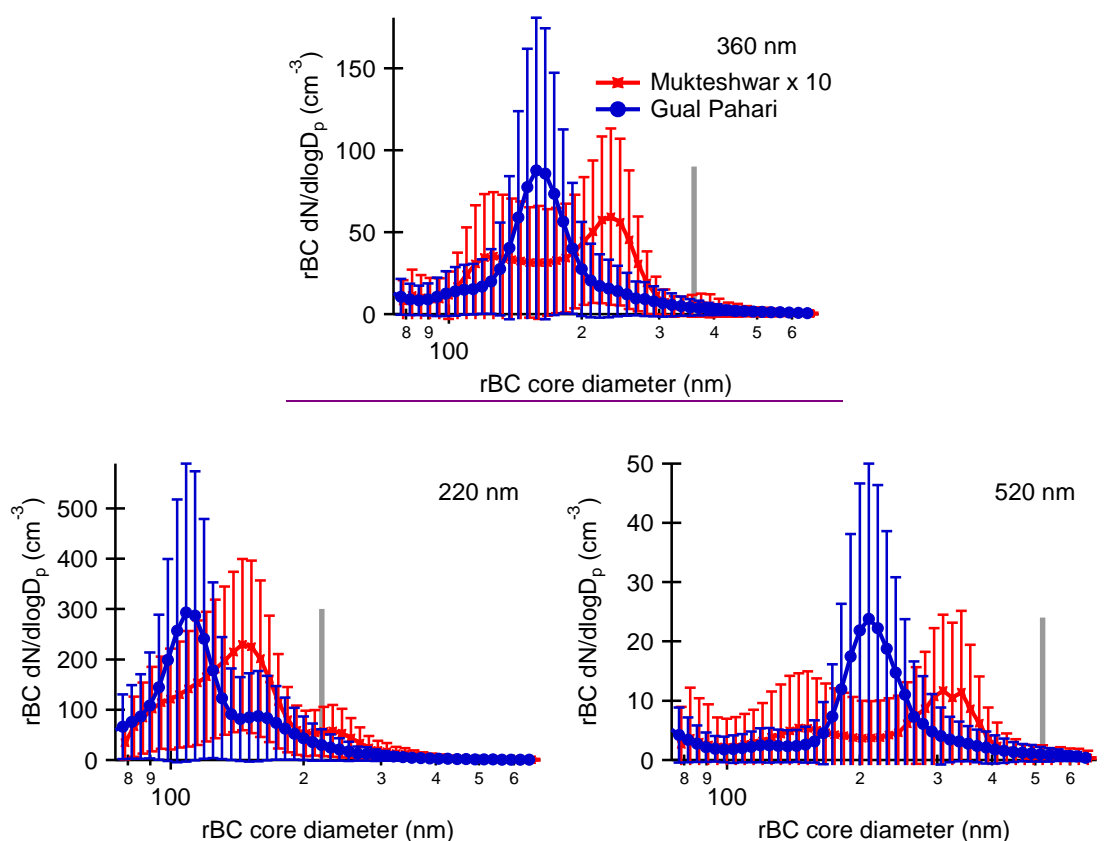


Figure S14: Campaign average rBC core number size distributions for 220, 360 and 520 nm DMA-selected mobility diameters (indicated by the vertical gray lines) from Mukteshwar (multiplied by a factor of ten) and Gual Pahari.

Refractory black carbon size mass and number distributions as a function of rBC core volume equivalent diameter are shown in the main text (Fig. 4). Figure S159 shows rBC and total particle number and mass size distributions measured by the SP2 and DMPS as a function of the DMA-selected mobility diameter.

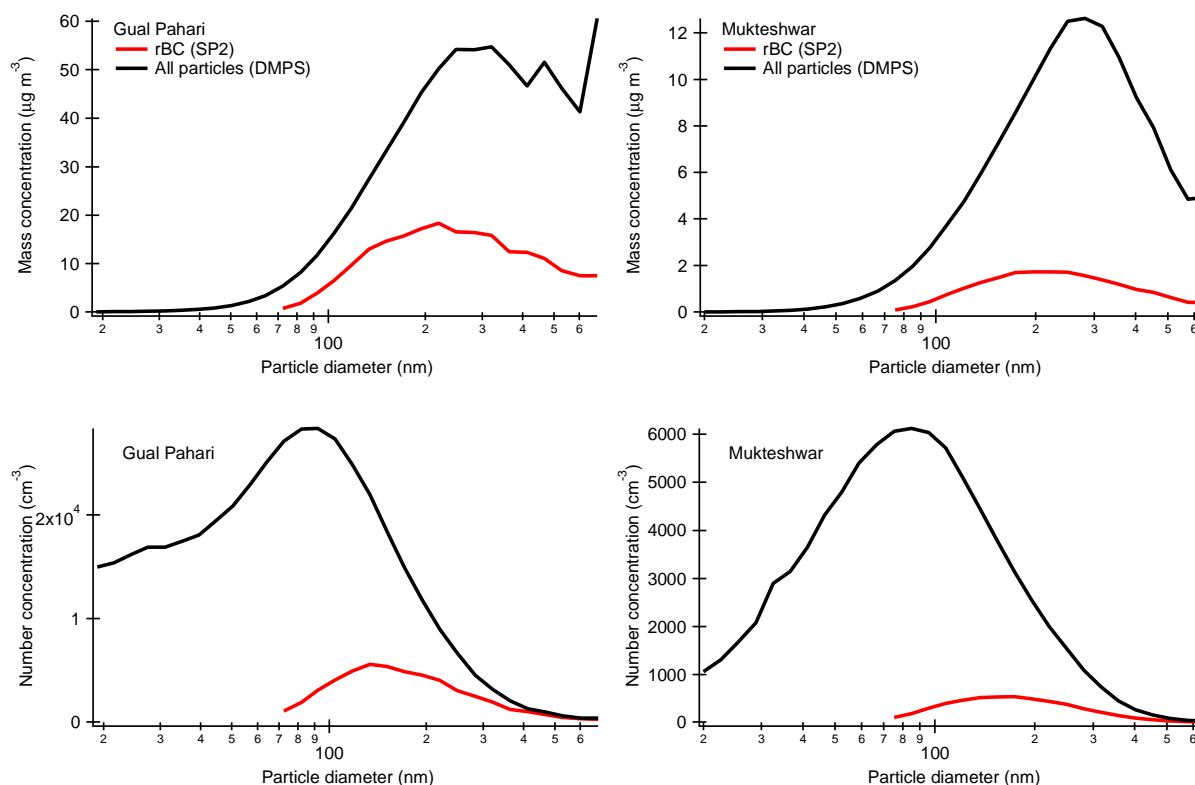


Figure S159: Total and rBC mass and number size distributions measured by the DMPS and SP2 for Gual Pahari and Mukteshwar. The volume distributions measured by the DMPS have been converted to mass by using 1000 kg m^{-3} particle density.

LEO analysis was conducted as described in the main text. Time series of the particles sizes (number average for each hour and mobility size bin) were calculated for different particle types (with and without rBC). Although the LEO method seems to work well for particles without rBC, examination of the chamber temperature dependency reveals problems with rBC-containing particles. Figure S16 shows the dependency of the LEO-derived optical particle size on the SP2 chamber temperature for particles without (top) and with rBC (bottom) for the 360 nm mobility size bin. When the size for non-rBC particles is independent if the instrument temperature, this is not the case for rBC-containing particles. The exact reason for this dependency is unknown, but an unusual sinusoidal noise signal seen on top of the Gaussian scattering signal seem to disturb the LEO fit especially at chamber temperature below $30 \text{ }^\circ\text{C}$. For this reason, LEO results are presented briefly in the main text (only averages for the 360 nm mobility size and when chamber temperature is at least $30 \text{ }^\circ\text{C}$).

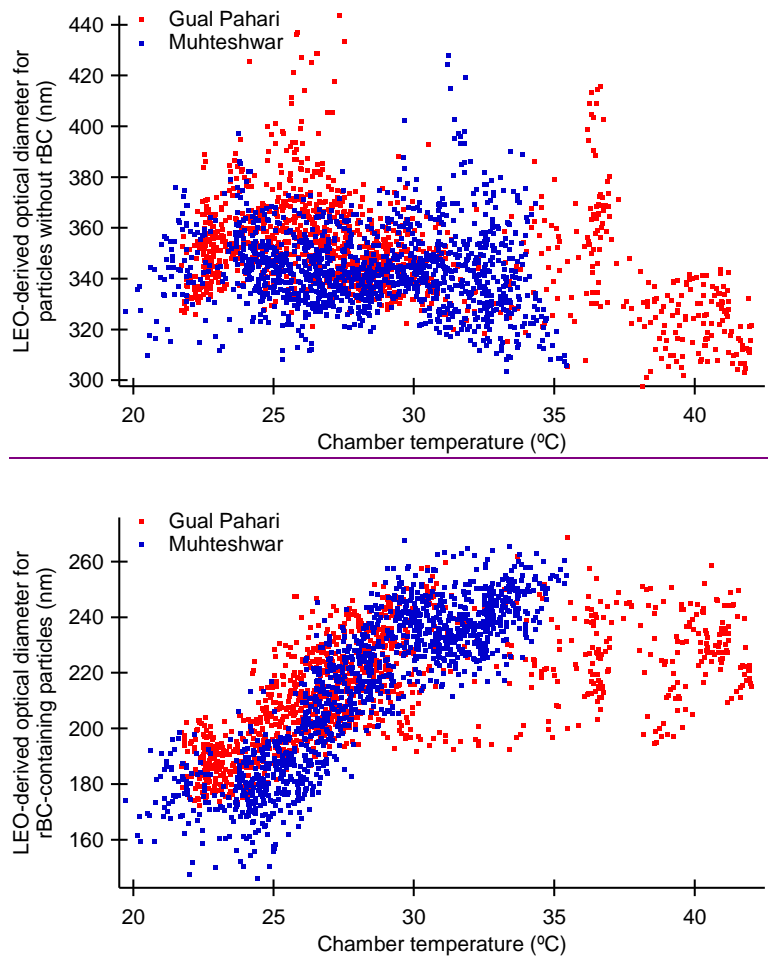


Figure S16: LEO-derived optical particle sizes as a function of chamber temperature for the 360 nm mobility size bin. The top graph is for particles without rBC and the bottom graph is for rBC-containing particles. Clear outliers are not shown.

~~In addition to the average rBC mass size distributions (total mass and geometric mass mean diameter and standard deviation) and mixing state (number and volume mean core diameters, those normalized by the mobility size, and number fraction of particles containing rBC) parameters for the 360 nm mobility size bins given in the main text (Table 1), figures S10 and S11 show the time series of these parameters (except number and volume mean core diameters as these are proportional to the normalized values).~~

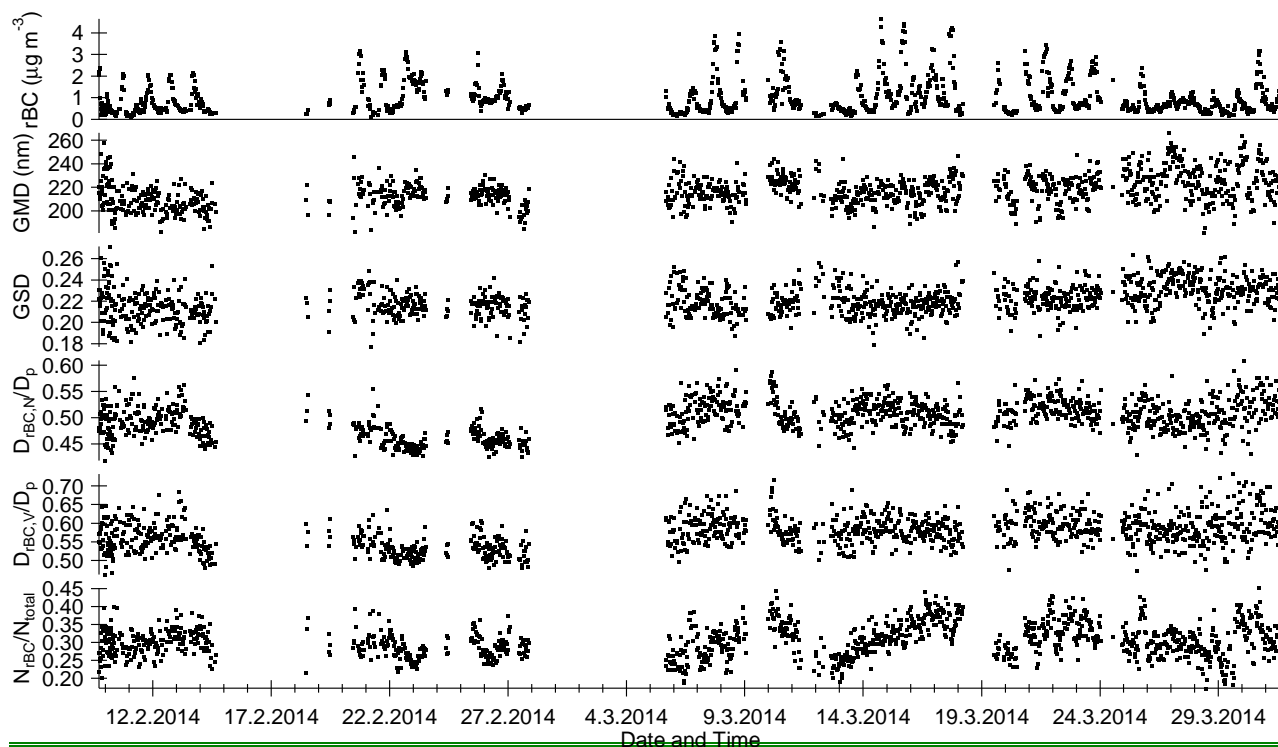


Figure S10: Time-series of the measured rBC mass-size distribution parameters (total rBC concentration and geometric mass mean diameter and standard deviation) and mixing state parameters (rBC core volume equivalent diameter (both number and volume averages) to particle diameter ratio and number fraction of particles containing rBC) for Mukteshwar.

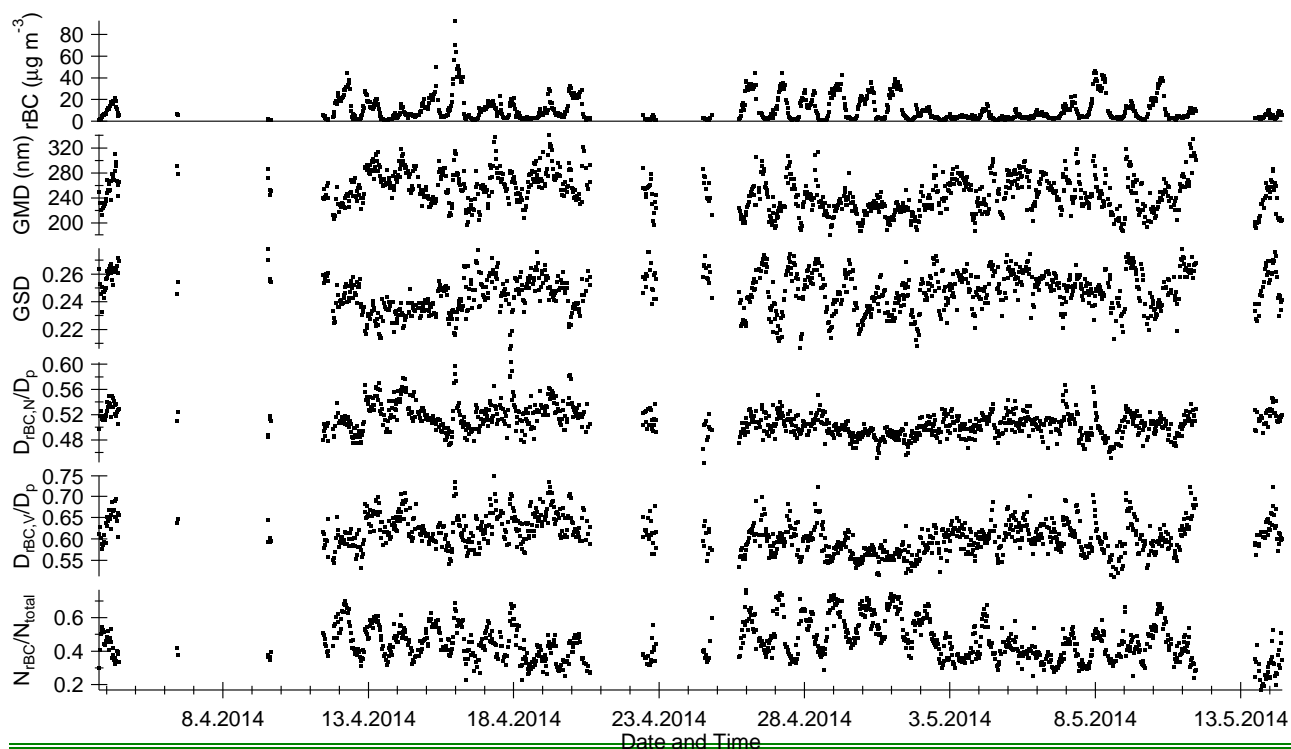


Figure S11: Same as Fig. S10, but for Gual Pahari

5 References

- Baumgardner, D., Popovicheva, O., Allan, J., Bernardoni, V., Cao, J., Cavalli, F., Cozic, J., Diapouli, E., Eleftheriadis, K., Genberg, P. J., Gonzalez, C., Gysel, M., John, A., Kirchstetter, T. W., Kuhlbusch, T. A. J., Laborde, M., Lack, D., Müller, T., Niessner, R., Petzold, A., Piazzalunga, A., Putaud, J. P., Schwarz, J., Sheridan, P., Subramanian, R., Swietlicki, E., Valli, G., Vecchi, R., and Viana, M.: Soot reference materials for instrument calibration and intercomparisons: a workshop summary with recommendations, *Atmos. Meas. Tech.*, 5, 1869-1887, 2012.
- Gysel, M., Laborde, M., Olfert, J. S., Subramanian, R., and Gröhn, A. J.: Effective density of Aquadag and fullerene soot black carbon reference materials used for SP2 calibration, *Atmos. Meas. Tech.*, 4, 2851–2858, 2011.
- Hansen, A., Rosen, H., and Novakov, T.: The aethalometer - An instrument for the real-time measurement of optical absorption by aerosol particles, *Sci. Total Environ.*, 36, 191-196, 1984.
- Hyvärinen, A.-P., Lihavainen, H., Komppula, M., Sharma, V. P., Kerminen, V.-M., Panwar, T. S., and Viisanen, Y.: Continuous measurements of optical properties of atmospheric aerosols in Mukteshwar, northern India, *J. Geophys. Res.*, 114, D08207, 2009.
- Kondo, Y., Sahu L., Moteki, N., Khan, F., Takegawa, N., Liu, X., Koike, M., and Miyakawa T.: Consistency and Traceability of Black Carbon Measurements Made by Laser-Induced Incandescence, Thermal-Optical Transmittance, and Filter-Based Photo-Absorption Techniques, *Aerosol Sci. Technol.*, 45, 295-312, 2011.
- Laborde, M., Schnaiter, M., Linke, C., Saathoff, H., Naumann, K.-H., Möhler, O., Berlenz, S., Wagner, U., Taylor, J. W., Liu, D., Flynn, M., Allan, J. D., Coe, H., Heimerl, K., Dahlkötter, F., Weinzierl, B., Wollny, A. G., Zanatta, M., Cozic, J., Laj, P., Hitznerberger, R., Schwarz, J. P., and Gysel, M.: Single Particle Soot Photometer intercomparison at the AIDA chamber, *Atmos. Meas. Tech.*, 5, 3077-3097, doi:10.5194/amt-5-3077-2012, 2012.
- Moteki, N., and Kondo, Y.: Dependence of Laser-Induced Incandescence on Physical Properties of Black Carbon Aerosols: Measurements and Theoretical Interpretation, *Aerosol Sci. Technol.*, 44, 663-675, 2010.
- Weingartner, E., Saathoff, H., Schnaiter, M., Streit, N., Bitnar, B., and Baltensperger, U.: Absorption of light by soot particles: determination of the absorption coefficient by means of aethalometers, *J. Aerosol Sci.*, 34, 1445-1463, 2003.
- Wiedensohler, A., Birmili, W., Nowak, A., Sonntag, A., Weinhold, K., Merkel, M., Wehner, B., Tuch, T., Pfeifer, S., Fiebig, M., Fjåraa, A. M., Asmi, E., Sellegri, K., Depuy, R., Venzac, H., Villani, P., Laj, P., Aalto, P., Ogren, J. A., Swietlicki, E., Williams, P., Roldin, P., Quincey, P., Hüglin, C., Fierz-Schmidhauser, R., Gysel, M., Weingartner, E., Riccobono, F., Santos, S., Gruning, C., Faloon, K., Beddows, D., Harrison, R., Monahan, C., Jennings, S. G., O'Dowd, C. D., Marinoni, A., Horn, H.-G., Keck, L., Jiang, J., Scheckman, J., McMurry, P. H., Deng, Z., Zhao, C. S., Moerman, M., Henzing, B., de Leeuw, G., Löschau, G., and Bastian, S.: Mobility particle size spectrometers: harmonization of technical standards and data structure to facilitate high quality long-term observations of atmospheric particle number size distributions, *Atmos. Meas. Tech.*, 5, 657-685, doi:10.5194/amt-5-657-2012, 2012.